学位論文(要約)

Developmental Mechanisms and Evolution of Shell Formation in Mollusca

(軟体動物における貝殻形成の発生メカニズムと進化)

平成 25 年 12 月博士（理学）申請

東京大学大学院理学系研究科

地球惑星科学専攻

清水　啓介

Abstract

A variety of animal morphology evolved in a long time, and the fossil record provides the only direct evidence of how the past life looked like. The morphological diversity is produced by developmental processes, which are difficult to reconstruct only from the fossil forms. In molluscs, their various shell shapes have evolved ever since the Cambrian, but their developmental processes remain unclear. In order to understand how various shell shapes are formed and have evolved in molluscs, I sought to reveal the molecular basis of initial shell formation and subsequent shell growth in embryos and adults using living species, and reached the following conclusions described in five chapters.

First, I examined expression patterns of the *decapentaplegic* (*dpp*) gene in the pond snail *Lymnaea stagnalis*, and analyzed the functions of *dpp* using the Dpp signal inhibitor dorsomorphin in order to understand developmental mechanisms and evolution of shell formation in gastropods (chapter 2). In the dextral snails, the *dpp* gene is expressed in the right half of the circular area around the shell gland at the trochophore stage and at the right-hand side of the mantle at the veliger stage. Two types of shell malformations were observed when the Dpp signals were inhibited by dorsomorphin. When the embryos were treated with dorsomorphin at the 2-cell and blastula stage before the shell gland is formed, the juvenile shells grew imperfectly and were not mineralized. On the other hand, when treated at the trochophore and veliger stages after the shell gland formation, juvenile shells grew to show a cone-like form rather than a normal coiled form. These results indicated that *dpp* plays important roles in the initial formation and subsequent coiling of the shell in this gastropod species.

Second, I compared expression patterns of the *dpp* gene in the shell gland and mantle tissues at various developmental stages between coiled-shell and non-coiled-shell gastropods (chapter 3). I analyzed the expression patterns of *dpp* for the two limpets *Patella vulgata* and *Nipponacmea fuscoviridis*, and for the dextral wild-type and sinistral mutant lineage of the pond snail *Lymnaea stagnalis*. The limpets exhibited symmetric expression patterns of *dpp* throughout ontogeny, whereas in the pond snail, the results indicated asymmetric and mirror image patterns between the dextral and sinistral lineages. I hypothesize that Dpp induces mantle expansion, and the presence of a left-right asymmetric gradient of the Dpp protein causes the formation of a coiled shell. This hypothesis provides a molecular explanation for shell coiling including new insights into post-embryonic shell development, and should aid in understanding how

various shell shapes are formed and have evolved in gastropods.

In chapters 2 and 3, I focused on the molecular basis of shell coiling in gastropods. However, coiled shell morphologies evolved not only in gastropods but also in cephalopods such as ammonoides and nautiloids. Thus, in chapter 4 as a first step to understand the molecular mechanism of shell coiling in cephalopod, I focused on Dpp expression patterns in the mantle of *Nautilus* and compared the patterns between gastropods and cephalopods. I revealed, using western blotting, that a Dpp signal gradient indeed exists in the mantle edge of the coiled-shell of not only gastropods but also *Nautilius*, and the gradient is in anterior-posterior direction in *Nautilius*. This pattern of Dpp signals correspondents with the shell growth gradient pattern like gastropod's results. Although coiled shell morphologies highly likely evolved independently in gastropods and cephalopods, the spiral shell growth appears to be regulated by the same molecular system using the asymmetric transmission of Dpp signals along the left-right or anterior-posterior axis.

Next in chapter 5, I sought to understand the role of the homeotic gene *engrailed* in early shell development by focusing on retinoic acid signal pathway. I examined the expression patterns of RA metabolizing enzyme *cyp26* in the limpet *Patella vulgate*, and found that *cyp26* is expressed around the edge of the shell field. As a result of gain or loss functional analysis of RA, shell deformation was observed in both gain and loss of RA analyses, and in both cases the shell failed to be calcified. Under both excess RA or RA shortage, *engrailed* is downregulated, and these results suggested that a modest concentration of RA is needed for the expression of *engrailed*, and that *engrailed* delimits the boundary of the shell forming area and regulates shell precipitation. These findings lead to an evolutionary hypothesis that the common ancestor of Mollusca likely used RA signaling system to produce the novel phenotypic trait that is called "shell" by recruiting the homeotic gene *engrailed*.

Finally, I described results of annotation for the signal molecule TGF-β superfamily genes, to which *dpp* belongs, using the recently determined draft genome sequence of the pearl oyster *Pinctada fucata* (in chapter 6). I found most of the representative genes and their paralogs of major signaling pathways involved in axial patterning, as well as several TGF-β superfamily genes which were hither to unknown in ptoyostome model organisms (*Drosophila*, *C. elegans*), such as BMP3, BMP9/10 and Nodal. By phylogenetic character mapping, I deduced a possible evolutionary scenario of the signaling molecules in the protostomes, and reconstructed the possible copy number of signaling molecule-coding genes in the

ancestral protostome. This ancestral reconstruction suggested a possibility that *P. fucata* retains the ancestral protostome conditions, giving further justifications to utilize this animal as a model organism for understanding developmental mechanisms of not only molluscan shell developmental formation but also lophotrochozoan body plan formation.

Abstract (Japanese)

生物の多様な形態は長い時間をかけて進化してきた。そして、化石は過去の生物が持っていた形質などに関する唯一の直接的証拠であり、化石を用いることで現生の生物からは推定することができない形態進化の変遷を復元することができる。軟体動物の貝殻は化石記録が豊富であるため、その形態進化に着目した進化古生物学的な研究は古くから行われてきた。しかし、実際の進化は発生プロセスの進化であり、化石として残る形態情報からだけでは形態進化の至近要因に迫ることは難しい。そこで、現生の貝類の貝殻形成および成長の発生プロセスに着目することで、貝殻の形態進化をもたらす分子メカニズムを明らかにし、化石を含む貝殻の多様な形態進化を理解することを目的とし、以下５つの研究を行った。

まず初めに、巻貝の貝殻形成の分子メカニズムと進化を明らかにするため、淡水棲巻貝の右巻種であるタケノコモノアラガイ（*Lymnaea stagnalis*）の *decapentaplegic*（*dpp*）の 遺伝子発現解析と Dpp のシグナル阻害剤を用いた機能解析を行った（第二章)。遺伝子 *dpp* は、モノアラガイのトロコフォア期に貝殻の初期形成を担う貝殻腺の右側でのみ発現することが知られている（Iijima et al. 2008)。今回、新たにベリジャー期における発現解析を行った結果、貝殻の後期成長を担う外套膜の右側の局所部分で発現していることを明らかにした。また、貝殻形成が開始されるトロコフォア期やベリジャー期において、Dpp のシグナル阻害剤ドルソモルフィンによる機能阻害実験を行なった結果, 貝殻が巻かずに円錐形の貝殻を持つ奇形が得られた。これらの結果は、Dpp の濃度勾配が貝殻の成長勾配を生み出し、外套膜上での *dpp* の発現パターンの変化が貝殻形態の進化を引き起こしている可能性を示唆した。

次に第三章では、貝殻の螺旋成長の進化を引き起こす発生メカニズムを探るため、貝殻が螺旋状に巻くタケノコモノアラガイ(*L. stagnalis*)の右巻（野生系統）と左巻（変異系統)、また、笠型の貝殻を持つセイヨウカサガイ（*Patella vulgata*）とクサイロアオガイ(*Nipponacmea fuscoviridis*)の様々な発生段階における *dpp* の発現解析を行い、それらの発現パターンを比較した。その結果、貝殻腺だけでなく外套膜においても、*dpp* がモノアラガイの右巻では右側、左巻では左側で発現するのに対し、笠型のセイヨウカサガイおよびクサイロアオガイでは左右対称に発現していることを明らかにした。さらに、Dpp シグナルの下流で働くリン酸化 SMAD1/5/8（pSMAD1/5/8）の発現解析を行なった結果、タケノコモノアラガイの右巻では外套膜の右側で、左巻では左側で強く発現するのに対し、セイヨウカサガイでは左右で発現量に差が見られなかった。これらの結果

から、外套膜上での *dpp* の発現パターンを左右非対称から左右対称へと変化させるような発生システムの変更によって外套膜の成長パターンが変化し、巻貝の貝殻形態を螺旋型から笠型への進化を引き起こしている可能性が示唆された。

螺旋型の貝殻形態は巻貝だけではなく、アンモナイトやオウムガイを含む頭足類においても進化した形質のひとつである。そこで第四章では、現生で唯一の外殻性頭足類であるオウムガイ(*Nautilus pompilius*)を用いて、巻貝の螺旋成長に重要な Dpp の下流で働くリン酸化 SMAD1/5/8（pSMAD1/5/8）の発現解析を行なった。その結果、前後方向に螺旋成長をするオウムガイの成体外套膜において pSMAD1/5/8 が前方で強く発現しており、Dpp シグナルの分布パターンが貝殻の成長勾配のパターンと一致していることが明らかとなった。Dpp の発現パターンが腹足類だけでなく、頭足類においても貝殻の成長パターンと一致していることから、腹足類と頭足類の共通祖先ですでに貝殻成長における Dpp の機能が獲得されていたことが示唆された。また、外套膜における Dpp シグナルの濃度勾配で生み出された貝殻の成長勾配のパターンの変更により、絶滅種であるアンモナイト類などの多様な貝殻形態の進化が引き起こされていた可能性が示唆される。

次に第五章では、貝殻の初期形成の分子メカニズムに着目した。ホメオティック遺伝子のひとつである *engrailed* は貝殻腺で発現することが軟体動物の多くの分類群において既に報告されており、貝殻形成領域の決定に重要であることが示唆されてきたが、実際の機能は不明であった。そこで、ホメオティック遺伝子を制御していることが期待されるレチノイン酸経路に関わる 2 つの遺伝子、レチノイン酸合成酵素(*aldh1a*)、レチノイン酸分解酵素(*cyp26*)を同定した。 また、セイヨウカサガイ(*P. vulgata*)のトロコフォア期・ベリジャー期において *cyp26* の発現解析を行った結果、貝殻腺と外套膜の縁辺部での発現が確認された。さらに、クサイロアオガイ(*N. fuscoviridis*)の初期胚にレチノイン酸またはレチノイン酸阻害剤で処理を行なった結果、貝殻腺で発現するホメオティック遺伝子である *engrailed* の発現が抑制され、貝殻が小さく、石灰化が起こらない表現型が観察された。これらの結果は、レチノイン酸経路が発生初期の形態形成を上流で制御するホメオティック遺伝子 *engrailed* を制御することで、軟体動物における貝殻という新規形質の獲得に重要な役割を果たしたという可能性を示唆している。

最後に、軟体動物における貝殻形成に重要な遺伝子である *dpp* を含むシグナル分子 TGF-β スーパーファミリーの進化プロセスを明らかにするため、近年明らかになった二枚貝類のアコヤガイ（*Pinctada fucata*）のゲノム情報から TGF-β スーパーファミリーに含まれる遺伝子の同定を行った。その結果、これまでショウジョウバエや線虫といった前口動物のモデル生物では見つから

なかった TGF-β スーパーファミリーの遺伝子（BMP3、BMP9/10、Nodal）を発見した。さらに、この結果と後口動物のゲノム情報をもとに、前口動物と後口動物の共通祖先における TGF-β スーパーファミリーの遺伝子セットの復元を行った結果、軟体動物には前口動物の祖先に近い遺伝子セットを保持していることが明らかとなった。今回得られた結果は、軟体動物の貝殻形成と進化の理解だけではなく、冠輪動物のボディープランの進化を理解する上で非常に重要である。

Contents

Chapter Ⅰ

General Introduction

本章については、5年以内に 雑誌等で刊行予定のため、非公開。

本章については、5 年以内に 雑誌等で刊行予定のため、非公開。

本章については、5 年以内に 雑誌等で刊行予定のため、非公開。

本章については、5 年以内に 雑誌等で刊行予定のため、非公開。

本章については、5年以内に 雑誌等で刊行予定のため、非公開。

本章については、5 年以内に 雑誌等で刊行予定のため、非公開。

本章については、5 年以内に 雑誌等で刊行予定のため、非公開。

本章については、5 年以内に 雑誌等で刊行予定のため、非公開。

Chapter Ⅱ
Possible Functions of Dpp in Gastropod Shell Formation and Shell Coiling

2. 1 Introduction

Shell is one of the main features of molluscs and is often preserved as fossils throughout geological time. The origins of molluscan shells probably date back to the late Precambrian (Runnegar 1996). Since then, shell has become greatly diversified in morphology.

In the pulmonate gastropod *Lymnaea stagnalis*, the late gastrula embryos develop a shell gland that is a secretory tissue formed by invagination of ectoderm cells. At the middle trochophore stage, a shell begins to be formed (Meshcheryakov 1990), and then, the mantle is developed at the veliger stage. After this stage, shell is formed by the mantle instead of the shell gland.

The shell gland and mantle, therefore, are important for the shell formation, and many gene expression analyses have been performed to find genes that are specifically expressed in these tissues. Examples include *engrailed*, *Hox* and *dpp* genes, which showed a specific pattern in some examined mollusc species. Dpp is a secreted polypeptide, belonging to the transforming growth factor-β (TGF-β) family. *dpp* is the invertebrate homolog of the genes of bone morphogenetic proteins BMP2 and 4 that play roles in bone formation in vertebrates. Like *engrailed* and *Hox*, *dpp* has been shown to be expressed in the shell forming area in gastropods and bivalves (Nederbragt et al. 2002; Iijima et al. 2008; Kin et al. 2009). In the limpet *Patella vulgata*, *dpp* is expressed in the circular area around the shell forming cells (Nederbragt et al. 2002). Interestingly, in the dextral snail *Lymnaea stagnalis*, this gene is expressed only in the right half part of the area around the shell forming cells (Iijima et al.

2008). This asymmetrical expression pattern of *L. stagnalis* suggested that *dpp* is associated with the signal pathway of the shell growth chirality: to make a coiling shell, the outer part of the shell must grow faster than the inner part.

In vivo functional analyses of these genes are essential for understanding the molecular mechanisms of shell formation. For *dpp*, Kin et al. (2009) reported results of gain of function analysis in the bivalve *Saccostrea kegaki* and suggested that this gene is important for establishing the characteristic shape of the bivalve shells.

In this paper, I performed a loss of functional analysis using a Dpp signal inhibitor in order to understand the roles of *dpp* in shell formation in the gastropod *Lymnaea stagnalis*. I also examined whether or not *dpp* is related to shell mineralization. My results indicated that *dpp* is associated with the development of the shell and the coiling growth of the shell in *Lymnaea stagnalis*.

2. 2 Materials and Methods

2. 2. 1 Animals

Individuals of *Lymnaea stagnalis* were reared in tap water in the laboratory. They lay eggs in capsules coated by jelly throughout the year. Eggs were collected and separated from their jelly by rolling the capsules on a sheet of paper (COMFORT service towel, NIPPON PAPER CRECIA, Tokyo, Japan), and incubated at 25ºC in sterilized tap water using 6-well dishes (BD Bioscience, NJ, USA).

2. 2. 2 Chemical treatment

To investigate the function of Dpp signaling in shell formation in snails, I exposed embryos to the chemical inhibitor, dorsomorphin. Eggs of *L. stagnalis* were incubated in sterilized tap water containing 0.1% DMSO (v/v) and dorsomorphin (6-[4-(2-Piperidin-1-ylethoxy) phenyl]-3-pyridin-4-ylpyrazolo [1,5-a] pyrimidine, Sigma-Aldrich Japan, Tokyo, Japan) at concentrations of 0.5 μM, 1 μM, 5 μM and 10 μM (each solution was diluted from 0.5 mM, 1 mM, 5 mM and 10 mM stock solutions of dorsomorphin in DMSO, respectively).

Eggs of *L. stagnalis* were also treated with rapamycin that interferes with the cellular metabolic machinery modifying cell growth and proliferation, and is known to have no effect on Dpp signaling. Eggs were incubated in sterilized tap water containing 0.1% DMSO and rapamycin (Sigma) at a concentration of 10 μM solution diluted from a 10 mM stock solution of rapamycin in DMSO. I treated embryos with dorsomorphin or rapamycin at 6 different developmental stages (2-cell, blastula, gastrula, trochophore, veliger and juvenile stages). As a negative control, embryos were also exposed to an aqueous solution of 0.1% DMSO. All control and drug-treated eggs were kept in the solutions in the dark at 25ºC for 10 days.

2. 2. 3 **in situ *hybridization***

Digoxigenin (DIG) - labeled sense and antisense RNA probes were synthesized for *dpp* from the clone that was prepared previously (Iijima et al. 2008) using the DIG RNA labeling Kit [SP6/T7] (Roche Diagnostics, Tokyo, Japan). The embryos were dechorionated using glass needles and tweezers under a microscope. Embryos were washed with PBT (final concentration: 0.1M NaCl, 7.7 mM Na_2HPO_4, 2.3 mM NaH_2PO_4, 0.1% Tween 20 (v/v), pH 7.4), and then fixed with 4% paraformaldehyde in PBT for 2 hours. After fixation, the samples were washed in PBT for 5 min at room temperature three times, followed by the dehydration with a gradual series of methanol/PBT (25/75, 50/50, 80/20) for 10 min each, and stored in 80% methanol at -20ºC.

In situ hybridization was conducted by referring to Nederbrgt et al. (2002) and Iijima et al. (2008). Embryos were dehydrated in a gradual series of methanol/PBT (80/20, 50/50, 25/75, 0/100), 15 min each. They were then treated with proteinase K in PBT (2 μg/ml) at room temperature and refixed in 4% paraformaldehyde as described above. Prehybridization was done for 1 hour at 60ºC, and hybridization was performed with digoxigenin-labeled probes in a hybridization buffer (50% formamide, 5×SSC, 5×Denhart's solution, 250 μg/ml Baker's yeast tRNA, 500 μg/ml sermon's sperm DNA) for overnight at 60ºC. After hybridization, the embryos were washed in PBT for 20 min twice at 60ºC and for 20 min twice at room temperature, and then treated with RNase A (20 μg/ml in 10 mM Tris buffer containing 0.5 M NaCl and 5 mM EDTA) for 30 min at 37ºC. RNase A was removed by washing the embryos three times in PBT. The embryos were incubated in the blocking solution (1% Blocking reagent in PBT; Roche) for 2 hours at room temperature. The embryos were incubated with antibody solution (1: 3000 dilution of the anti-Digoxigenin-AP, Fab fragment in blocking buffer; Roche), and washed five times with PBT for 10 min each. Staining was performed with Nitro blue tetrazolium / 5-bromo-4-chloro-3-indolyphosphate p-toluidine salt

(NBT/BCIP) ready-to-use tablet (Roche) in distilled water (final concentration: 0.4 mg/ml NBT, 0.19 mg/ml BCIP, 100 mM Tris buffer, pH 9.5, 50 mM $MgSO_4$). When an adequate signal level was observed, embryos were washed three times in PBT and stored in 50% glycerol in PBT.

2. 2. 4 Scanning electron microscopy

The embryos were dechorionated using glass needles and tweezers under a microscope. Embryos were washed with PBT, and then fixed in 2.5% glutaraldehyde in PBS for 1 hour at room temperature. After fixation, embryos were dehydrated for 30 min each with a gradual series of ethanol/PBT (50/50, 70/30, 80/20, 90/10, 100/0). The ethanol was replaced by t-butylalcohol using a gradual series of ethanol/t-butylalcohol (50/50, 100/0, 100/0) for 15 min each. Samples in t-butylalcohol were freeze-dried and sputter-coated with platinum and palladium using an ion coater (E-1030, HITACHI), and observed under a scanning electron microscope (SEM, S-4500, HITACHI, Tokyo, Japan) at 15 kV.

2. 2. 5 Identification of shell mineralization

For the examination of the presence or absence of calcium in the larval shells, I used energy dispersive X-ray spectrometer (EDS, KEVEX). The samples were prepared as described above in the section for scanning electron microscopy. Analysis of elemental composition was done using Spot-mode at x1000 magnification for 60 seconds.

I also performed Raman spectroscopy using a micro-Raman measurement system (see details for Fukura et al., 2006). The samples were excited with an Ar ion laser (514.5 nm, 5500A, Ion Laser Technology, Utah, USA). The scattered light was detected using a Silicon-based charge-coupled device (CCD) camera with 1024 x 128 pixels (DU-401-BR-DD SH, Andor Technology, Belfast, Northern Ireland). The spectral resolution was approximately

1.5 cm^{-1} per pixel. The Raman spectra were measured for 10 seconds with the Ar ion laser (approximately 5 mW at the sample surface). The excitation laser beams were focused on a spheroidal spot of approximately 2 x 2 x 10 lm in volume using a 50 x objective lens. The samples of the trochophores, veligers, juveniles and adults were fixed with 4% paraformaldehyde in PBT and stored 4ºC in PBT prior to this analysis.

2. 3 Results

2. 3. 1 Mineralization in normal shells

The development of *L. stagnalis* examined in this study proceeded in very much the same way as described by previous studies (Morrill, 1982; Mecshcheryakov, 1990). At the late trochophore stage, a very small and thin shell is formed (Fig. 2. 1a, d), and then, the shell becomes bigger throughout the veliger and juvenile stages (Fig. 2. 1b, c, e, f). Those shells appeared to be mineralized when observed under a polarization microscopy (Fig. 2. 1d, e, f). The mantle begins to develop at the late veliger stage (Fig. 2. 2a-d). The shells of molluscs are composed of calcium carbonate and organic matrices that contain β-chitin, silk-fibroin and glycoproteins (Cartwright and Checa, 2007). I analyzed the components of the shells at the trochophore, veliger, juvenile and adult stages by Energy Dispersive X-ray Spectrometer (EDS). In the shells at the late trochophore and early veliger stages, the characteristic peak of the calcium element, around 3.60 keV, was not observed (Fig. 2. 2e, f). After the late veliger stage, calcium element was detected clearly (Fig. 2. 2g, h).

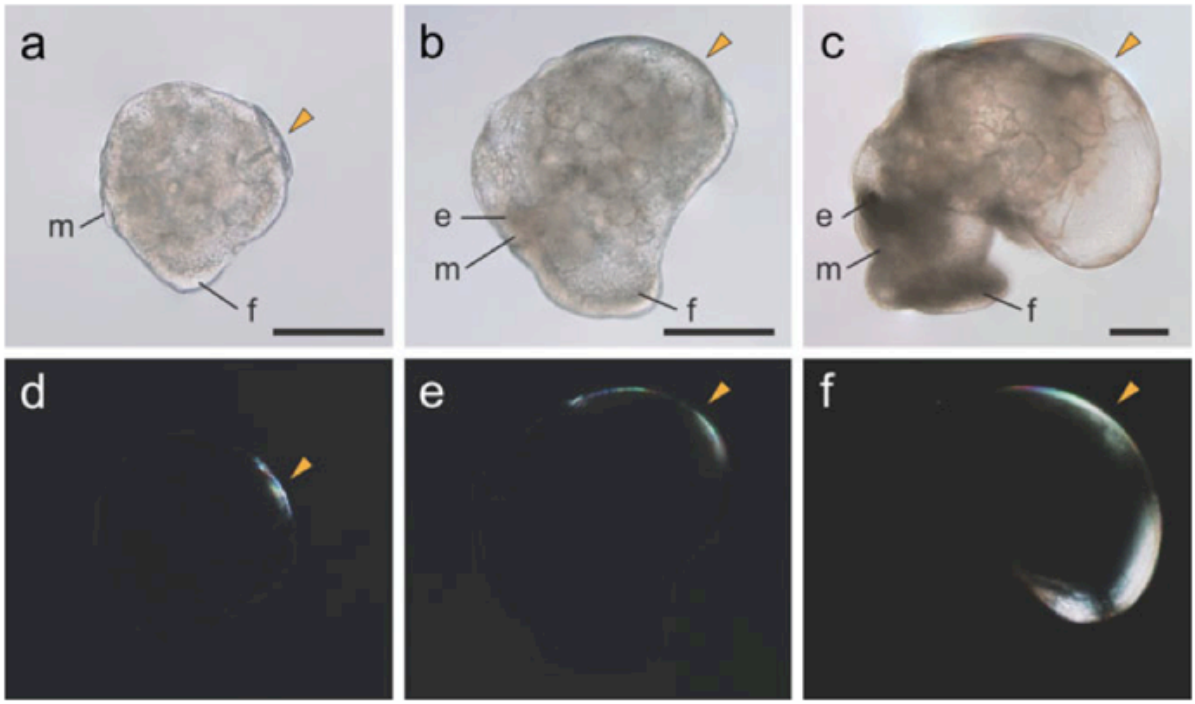

Fig. 2. 1 Shells of *L. stagnalis* at the trochophore, veliger and juvenile stages. a-c Bright field images. **d-f** Polarization images. Images **a-c** correspond to **d-f**, respectively. **a, d** Trochophore stage. **b, e** Veliger stage. **c, f** Juvenile stage. All images are viewed from the left side. **d-f** Bright area shows the shell indicated by orange arrowheads. *e*: eye, *f*: foot, *m*: mouth. Scale bar, 100 μm.

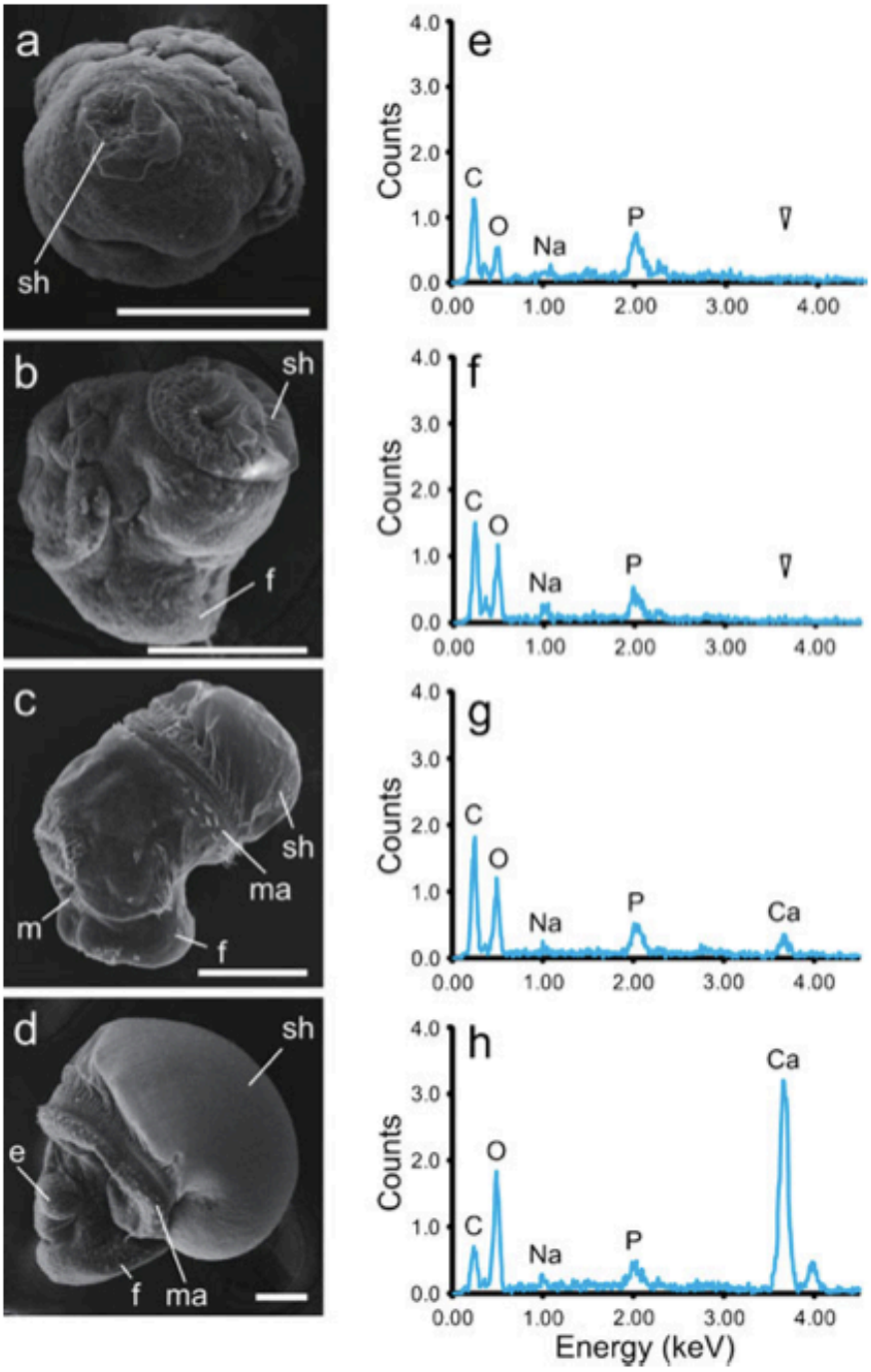

Figure 2. 2 SEM images (a-d) and the results of X-ray spectroscopy (e, f, g, h). a Trochophore stage viewed from the shell gland. **b** Left side view of the early veliger stage. **c** Left side view of the late veliger stage. **d** Left side view of the juvenile stage. (**e, f**) The specific calcium element peak (around 3.60 keV, white arrowheads) was not observe at the late trochophore and early veliger stages. (**g, h**) The specific calcium element peak was detected in the late veliger and juvenile stages. *e*: eye, *f*: foot, *m*: mouth, *ma*: mantle, *sh*: shell. Scale bars in **a-d**, 100 μm.

To examine the components of the unmineralized shells at the trochophore and veliger stages, I used Raman spectroscopy. From the shell of the late trochophore and early veliger stages, we could not detect any intense peak (Fig. 2. 3a, b). On the other hand, two peaks at 1121 and 1510 cm^{-1} were observed at the late veliger stage (Fig. 2. 3c). These two peaks do not correspond to calcium carbonates, but to the single and double carbon-carbon bonds, respectively (De Paula et al. 2010). Pulmonate snails including *L. stagnalis* are known to have an aragonitic shell (Bandel, 1990). At the juvenile and adult stages, two peaks of aragonite at 703 and 1085 cm^{-1} were observed as well as the peaks showing carbon-carbon bonds (Fig. 2. 3d, e). At these stages, calcium was also detected by EDS. In the adult shell that was treated with 1% bleach, only two peaks of aragonite were detected (Fig. 2. 3f).

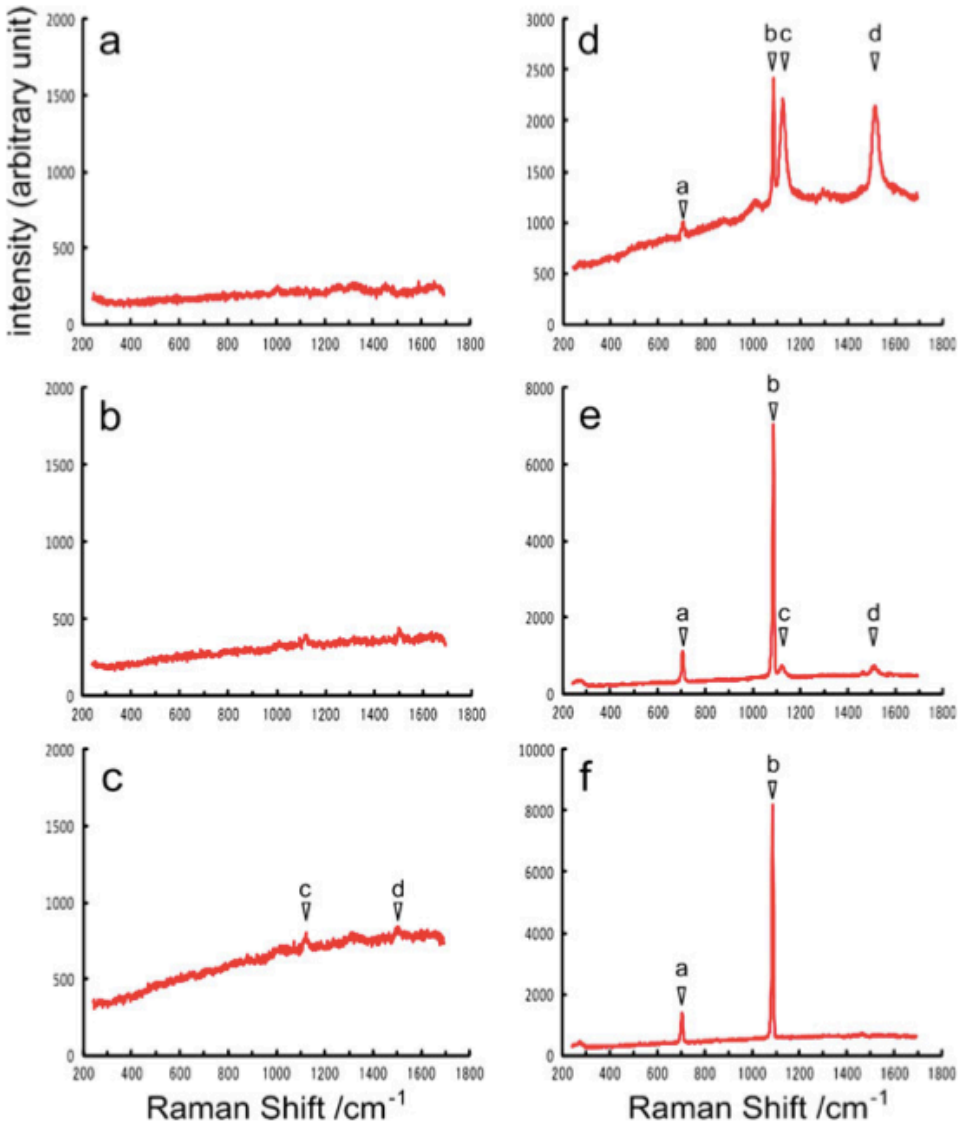

Figure 2. 3 Raman spectra of the shells (a The trochophore stage, b The early veliger stage, c The late veliger stage, d The juvenile stage, e, f The adult stage). e Adult shell treated by 1% bleach overnight. Four specific peaks corresponding to the following structures are indicated by white arrowheads: **a:** aragonite; 703 cm^{-1}, **b:** carbonate; 1085 cm^{-1}, **c, d:** polyen; 1121 and 1510 cm^{-1}.

2. 3. 2 Expression of Lstdpp in L. stagnalis

At the late trochophore stage, *Lstdpp* is expressed strongly only in the right half of the circular area around the shell gland (Fig. 2. 4a, b). This expression pattern is the same as observed in a previous study (Iijima et al. 2008). At the veliger stage, *Lstdpp* is expressed in the mantle as a small spot also in the right side only (Fig. 2. 4c, d).

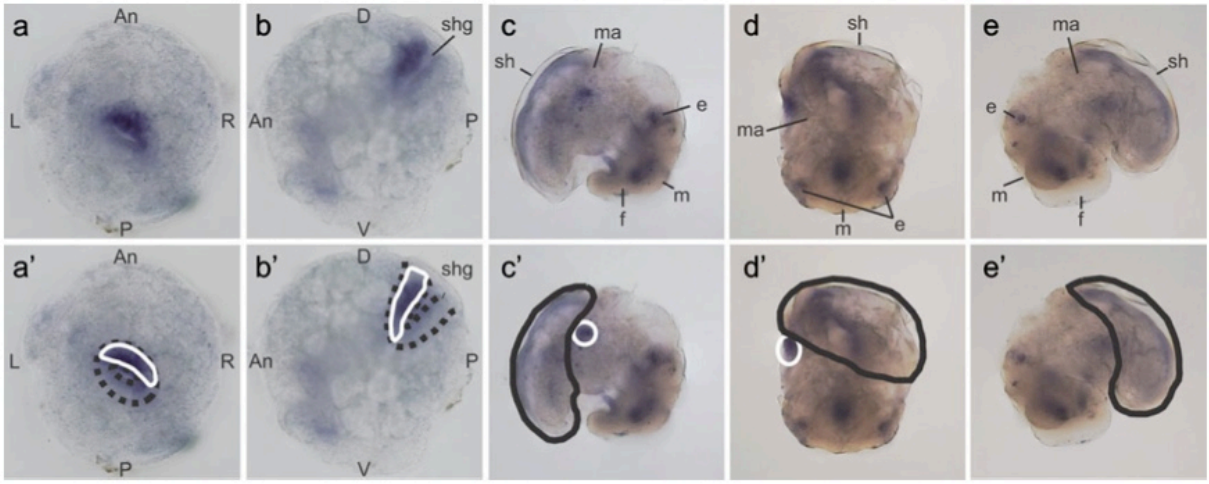

Figure 2. 4 Expression patterns of *Lstdpp* in the late trochophore (**a, b**) and veliger stage (**c, d, e**) of *L. stagnalis*. **a** shell gland view. **b, e** left side view. **c** right side view. **d** anterior view. **a', b'** Broken black lines indicate the shell gland and white lines indicate the *Lstdpp* expression. **c', d', e'** Black lines indicate the shells. **A, b** The expression of *Lstdpp* in the late trochophore stage is asymmetric in the shell gland. **c, d, e** In veliger stage, *Lstdpp* is expressed in arestricted spot in the right side of the mantle. *An*: anterior, *e*: eye, *f*: foot, *L*: left, *m*: mouth, *ma*: mantle, *P*: posterior, *R*: right, *sh*: shell, *shg*: shell gland opening.

2. 3. 3 Dorsomorphin treatment (Dpp inhibition)

About 250 embryos each at six different developmental stages (2-cell, blastula, gastrula, trochophore, veliger and juvenile stages) were exposed to dorsomorphin. Table 1 shows the frequencies of the normal and malformed forms in the individuals that grew to become juveniles. In normal development, a 7-day juvenile made the first helical turn of the shell (Fig. 2. 5a). Two types of shell malformation were observed only in the dorsomorphin-treated group, i.e., the immature shell (Fig. 2. 5b) and the non-coiled shell (Fig. 2. 5c). Other types of malformations were observed in both the control and the dorsomorphin-treated groups (Fig. 2. 5d, e, f). I categorized the malformations into two groups: the specific shell malformations caused by *dpp* inhibition (Sm) and the other unspecific malformations (Um) (Table 2. 1 and 2. 2). When embryos were treated with 0.5 μM dorsomorphin at early stages (the 2-cell and blastula stages), immature shells were produced at a significant level (Fig. 2. 6, statistical analysis by Fisher's exact test, 2-cell stage; $p<0.001$, blastula stage; $p<0.05$). I did not observe immature shells when embryos were exposed to dorsomorphin after the gastrula stage. Instead, the other type of shell malformations, or the non-coiled shell, was produced with the 1 μM dorsomorphin when treated at the trochophore and veliger stages (Fig. 2. 6, veliger stage; $p<0.001$, Fisher's exact test).

Table 2. 1a Phenotypes of the embryos treated with dorsomorphin.

Treatment stage	Concentration	N	Nomal Juveniles (%)	Malformed Juveniles (%)	Mortality (%)
2-cell stage	0 μM	2880	96.1	2.2	1.7
	0.5 μM	265	53.2	18.1	28.7
	1 μM	505	0.0	0.0	100.0
Blastula	0.5 μM	360	56.7	17.5	25.8
	1 μM	225	0.4	0.9	98.7
Gastrula	1 μM	274	87.2	10.2	2.6
	3 μM	140	0.0	0.0	100.0
Trochophore	1 μM	480	87.1	10.6	2.3
	5 μM	470	55.1	24.7	20.2
	10 μM	100	2.0	1.0	97.0
Veliger	1 μM	548	85.6	3.6	10.8
	5 μM	385	80.8	6.0	13.2
	10 μM	295	67.8	9.2	23.1
Juvenile	5 μM	290	96.2	3.1	0.7
	10 μM	290	89.3	2.8	7.9

Table 2. 1b Phenotypes of the malformed juveniles after dorsomorphin treatment.

Treatment stage	Concentration	N	Sm* (%)	Um* (%)
2-cell stage	0 μM	64	0.0	100.0
	0.5 μM	48	20.8	79.2
	1 μM	0	-	-
Blastula	0.5 μM	63	9.5	90.5
	1 μM	2	100.0	0.0
Gastrula	1 μM	28	0.0	100.0
	3 μM	0	-	-
Trochophore	1 μM	51	2.0	98.0
	5 μM	116	0.9	99.1
	10 μM	1	0.0	100.0
Veliger	1 μM	20	20.0	80.0
	5 μM	23	4.4	95.6
	10 μM	27	0.0	100.0
Juvenile	5 μM	9	0.0	100.0
	10 μM	8	0.0	100.0

* Sm means shell malformations and Um means unspecific malformations.

Table 2. 2 Phenotypes of the embryos treated with rapamycin.

Treatment stage	Concentration	N	Nomal Juveniles (%)	Malformed Juveniles (%)	Mortality (%)	Malformed Juveniles	
						Sm* (%)	Um* (%)
2-cell stage	10 μM	250	31.2	57.6	11.2	0.0	100.0
Blastula	10 μM	220	33.6	65.0	1.4	0.0	100.0
Gastrula	10 μM	212	75.0	24.1	0.9	0.0	100.0
Trochophore	10 μM	250	73.2	26.0	0.8	0.0	100.0
Veliger	10 μM	210	98.1	1.4	0.5	0.0	100.0

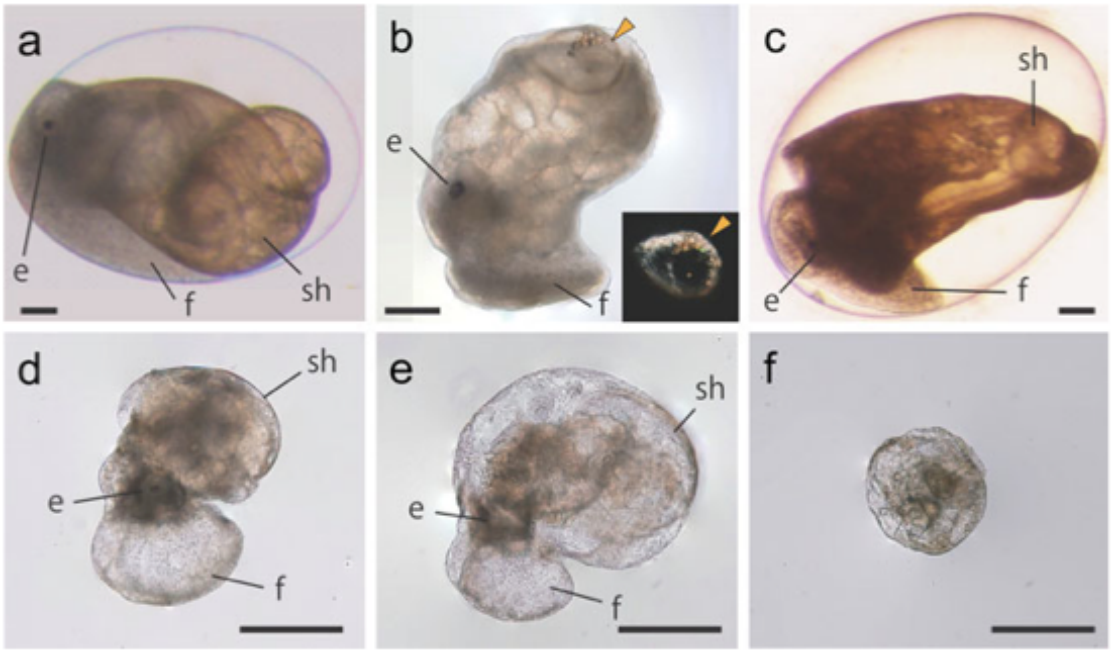

Figure 2. 5 Phenotypes of normal coiled and malformed juveniles observed in dorsomorphin treated and control groups. a-f Bright field images. **a** 7-day normal juvenile stage. **b, c** Shell malformations caused by dorsomorphin treatment. Immature shell phenotype (**b**) and non-coiled shell phenotype (**c**). Orange arrowheads show the shell (**b**). **d-f** Unspecific malformations arose from both the control and dorsomorphin treated groups. They have a swelled foot (**d**), swelled mantle (**e**), or a hydropic whole body (**f**). *e*: eye, *f*: foot, *ma*: mantle, *sh*: shell. Scale bar, 100 μm.

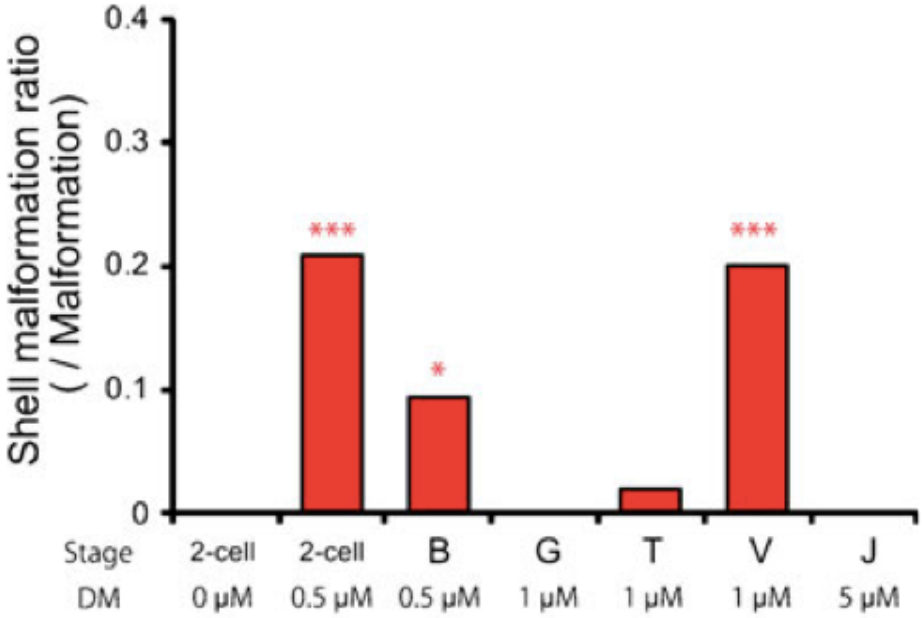

Figure 2. 6 The effect of dorsomorphin on shells observed at 7-day juvenile stage. Stage B, G, T, V and J indicate Blastula, Gastrula, Trochophore, Veliger and Juvenile stages. "0 µM dorsomorphin treated at 2-cell stage" means control group (0.1 % DMSO). The shell malformations were significantly produced by dorsomorphin treatment at the 2-cell and the veliger stages (Fisher's exact test; $p<0.001$), blastula stage (Fisher's exact test; $p<0.05$). This graph was produced using data from table 1b.

The embryos were also exposed to the rapamycin solution, which is an inhibitor of cell growth and proliferation (Grande and Patel, 2009). Some embryos treated with rapamycin indicated retarded development relative to normal ones, and did not hatch within 15 days after oviposition. Some others treated with rapamycin showed a swelled foot or mantle that formed a normal shell (Fig. 2. 5d, e, f, Table 2. 2). Some types of malformations (Fig. 2. 5d, e, f) occurred in the dorsomorphin treated group were also observed in the rapamycin treated group. Therefore, these malformations were considered not to be due to the inhibition of Dpp signaling.

2. 3. 4 Extent of mineralization of malformed "shells"

SEM observations revealed that the malformed shells by the dorsomorphin treatment are small, and accompanied by a not-well developed mantle (Fig. 2. 7a, b). To characterize the shell malformations in detail, we also analyzed the malformed shells using EDS and Raman spectroscopy. The EDS analysis indicated that those 'shells' contain little calcium, showing no characteristic peaks of calcium (Fig. 2. 7c). In these "shells", the aragonite and carbonate peaks at 703 and 1085 cm^{-1} were not observed by Raman spectroscopy (Fig. 2. 7d).

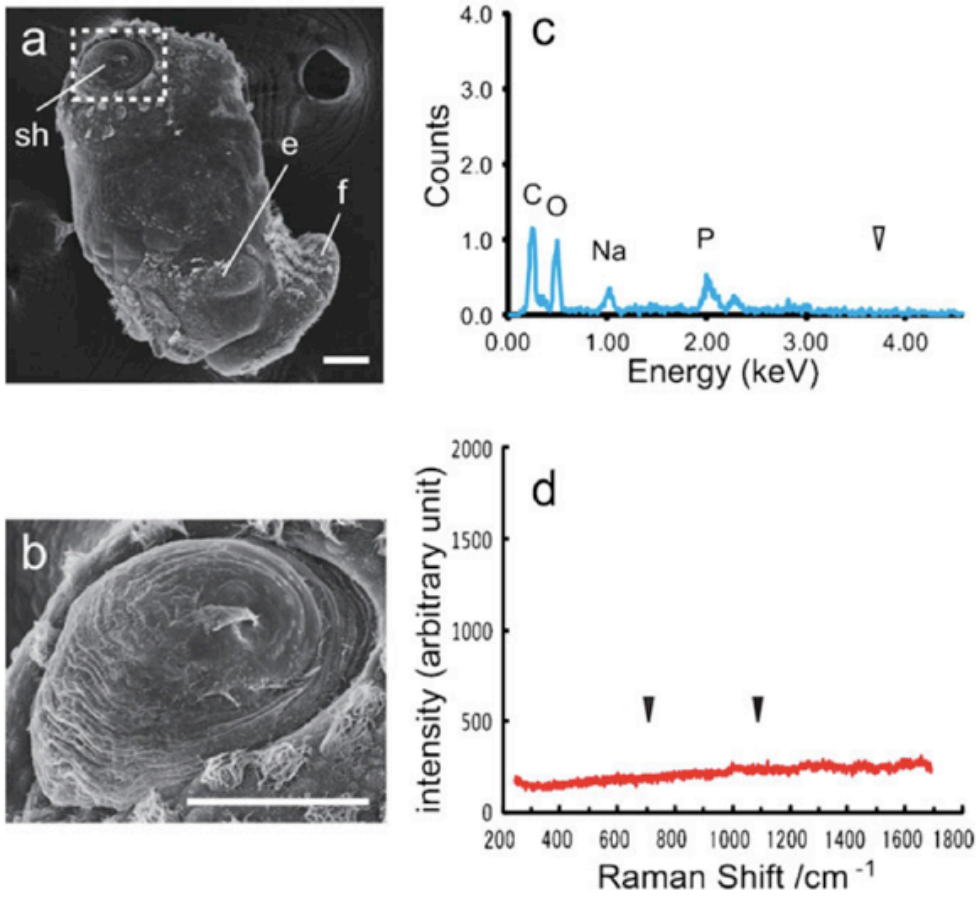

Figure 2. 7 SEM images, X-ray spectra and Raman spectra of the malformed immature shell. a The malformed shell viewed from left side. **b** Enlargement of the broken lines square in **a**. **c** A result of EDS analysis. The specific calcium element peak was not observed (white arrowhead). **d** A result of Raman spectroscopy on the malformed shell. Aragonite peaks (703 and 1085 cm^{-1}) were not observed (black arrowheads). *e*: eye, *f*: foot, *sh*: shell. Scale bars in **a, b**, 50 μm.

2. 4 Discussion

2. 4. 1 Shell formation in early development of gastropods

In the gastropod *Haliotis tuberculata*, the first larval shell was observed at the early trochophore stage, but this shell is not mineralized, and assumed to be a thin organic layer because no birefringence was observed under polarizing microscopy (Jardillier et al. 2008). It appears that the initial shell mineralization generally occurs at the pre-veliger stage in gastropods (Eyster and Morse 1984; Eyster 1986; Collin and Voltzow 1998; Jardillier et al. 2008).

In *Lymanaea stagnalis*, the shells at the trochophore and the early veliger stages show birefringence under polarizing microscopy (Fig. 2. 1d, e). However, the results of EDS analysis and Raman spectroscopy indicated that they are probably thin organic layers, and yet to be mineralized (Fig. 2. 2a, b, e, f, 3a, b). At the late veliger stage, the shell start to contain calcium (Fig. 2. 2c, g), but we could not detect the aragonite and carbonate peaks in the shells of late veligers by Raman spectroscopy (Fig. 2. 3c). These results suggest that the mineralization in the shells starts in the late veliger or early juvenile stage in *L. stagnalis* (Fig. 2. 2d, H, 3d, e). Therefore, the onset of mineralization is a little later than that of other gastropod species (Eyster and Morse 1984; Eyster 1986; Bielefeld and Becker 1991; Collin and Voltzow 1998; Jardillier et al. 2008). The initial mineralization is likely to be performed not by the shell gland, but by the mantle in *L. stagnalis*.

2. 4. 2 Function of dpp in shell formation

In gastropods, the expression pattern of *dpp* has been reported for a number of species (Lambert and Nagy, 2002; Nederbragt et al., 2002; Koop et al., 2007; Iijima et al., 2008), but the functions of this gene have not been clearly understood. Recently, the three dimensional structure of the intracellular kinase domain in the BMP (the vertebrate homolog of Dpp) type I receptors (Activin receptor type I precursor, *Hs*ACVR1) was resolved in *Homo sapience* (Chaikuad et al. 2009). Dorsomorphin is interlocked with the ATP binding pocket of the ACVR1 kinase domain, and the functionally important amino acid residues for this interaction have been clarified. Namely, His (293) is essential for the hydrogen bonding with dorsomorphin, and the six hydrophobic amino acids Val (214, 222), Leu (263, 343), Tyr (285) and Gly (289) are indispensable for the hydrophobic interaction with dorsomorphin. We compared the amino acids sequences of *Hs*ACVR1 and BMPR1 or BMPR1-like sequences among many animals, including the deuterostomes *H. sapience*, *Gallus gallus*, *Xenopus laevis*, *Danio rerio*, the ecdysozoans *Drosophila melanogaster*, *Caenorhabditis elegans*, and the lophotorochozoan *Crassostrea gigas* (Fig. 2. 8a). Dorsomorphin is expected to inhibit the BMP signal pathway not only in vertebrates but also in invertebrates including molluscs, because the seven amino acid residues essential for the binding with dorsomorphin are well conserved (Fig. 2. 8): Six residues are identical and the remaining one is different but similar in hydrophobicity (Val in human and Leu in oyster). It is therefore logical to assume that dorsomorphin will inhibit Dpp signaling in molluscus including *Lymnaea stagnalis*. In a recent study, it is indicated that dorsomorphin inhibits not only BMP signaling but also the pathway involving vascular endothelial growth factor (VEGF), (Cannon et al. 2010). It remains possible, therefore, that the effects of dorsomorphin we observed arouse from inhibition of the VEGF signaling. However, it appears likely that the effects we observed arose from blocking of the BMP pathway, because the phenotypes of the shell malformation

caused by dorsomorphin, as discussed below, indicate morphologies is exactly expected from the *dpp* expression patterns.

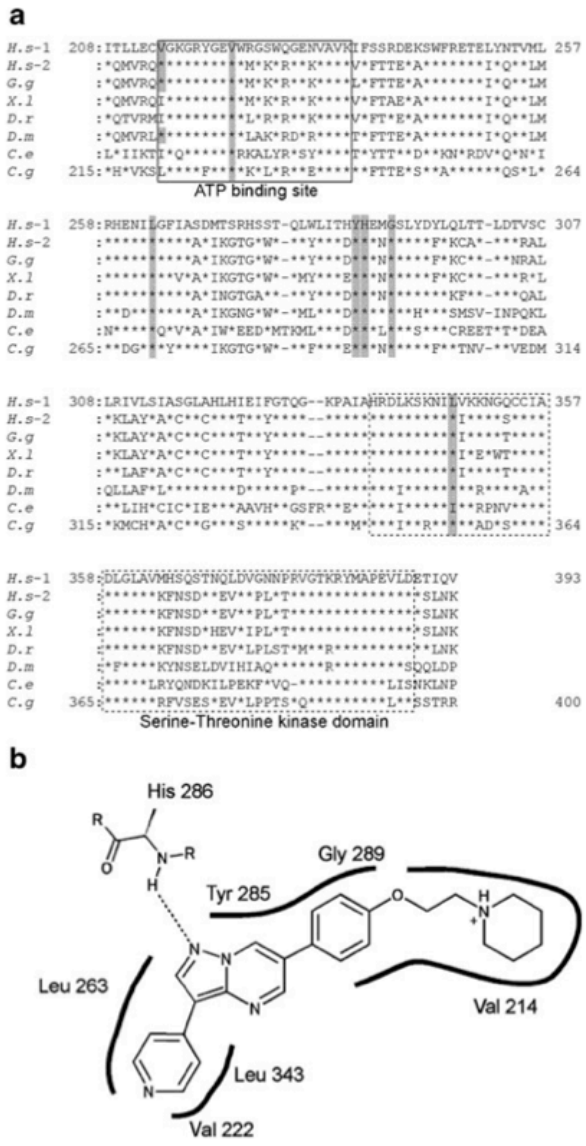

Figure 2. 8 a Aliment of the partial amino acids sequences of BMP type I receptors. Abbreviations: *H.s*-1, the sequence of activin receptor type I precursor (ACVR1) of *Homo sapiens* (NP_001104537); *H. s*-2, bone morphogenetic protein receptor type-1A (BMPR1A) of *H. sapiens* (NP_004320); *G. g,* BMPR1A of *Gallus gallus* (NP_990688); *X. l,* BMPR1A of *Xenopus laevis* (NP_001081209.1); *D. d,* BMPR1A of *Danio rerio* (NP_571696); *C. g,* BMPR1B of *Crassostrea gigas* (CAE11917); *D. m,* Thick vein of in *Drosophila melanogaster* (NP_787989); *C. e,* SMALL family member (sma-6) of *Caenorhabditis elegans* (NP_495271). The seven amino acid residues that are essential for the binding with dorsomorphin by molecular interaction are shown by shading. The ATP binding site, and the serine/threonine kinase domain are boxed by solid lines and broken lines, respectively. **b.** The schematic drawing of the binding between BMP type-I receptor and dorsomorphin based on Chaikuad et al. (2009). The broken line denotes the hydrogen bond, and bold lines indicate hydrophobic interactions. The seven amino acid residues of ACVR1 and BMPR1 that are essential for the interaction with dorsomorphin are shown with the residue number of the human ACVR1 sequence. They correspond to the shaded amino acids in Fig. 2. 8a.

I observed two types of shell malformations when the Dpp signal was inhibited by dorsomorphin (Fig. 2. 5b, c). When embryos were treated with dorsomorphin before the shell gland formation (the 2-cell and blastula stages), the mantle did not develop at all. Their shells are smaller than the normal shells (Fig. 2. 7a, b). Results of EDS analysis and Raman spectroscopy indicated that their "shells" contain little calcium (Fig. 2. 7c). Therefore the "shells" are uncalcified (Fig. 2. 7d) as in the normal shells of the trochophore and early veliger stages. These facts indicate that Dpp plays an important role in the mantle development, and consequently, the shell formation.

The other shell malformations, the non-coiled shells (Fig. 2. 5c), were observed when the embryos were treated with dorsomorphin after the shell gland formation at the trochophore and veliger stages. This phenotype is similar to a limpet shell, which shows a symmetrical shape. After the trochophore stage, *dpp* is expressed asymmetrically in the shell gland and mantle in normal individuals (Fig. 2. 4). These results collectively suggest that Dpp signals are associated with asymmetric growth of the mantle, controlling the process of shell coiling in *L. stagnalis*.

Similar-looking non-coiled shells were observed in a study that performed inhibition of Nodal signaling pathway in the gastropod *Biomphalaria glabrata* (Grande and Patel, 2009). The *nodal* gene is one of the famous genes that decide the left-right axis in the embryos (Lowe et al, 2001). In gastropods, the body handedness corresponds to the shell-coiling direction and to the *nodal* expression pattern, i.e. the *nodal* gene is expressed at the right side of the embryo in the dextral gastropod *Lymnaea stagnalis* (Kuroda et al., 2009). The non-coiled shells were produced by the Nodal inhibitor treatment before the blastula. But in *L. stagnalis*, this phenotype was observed only when embryos were treated with the Dpp inhibitor after the trochophore stage. Furthermore, the asymmetric *nodal* expression pattern is observed as early as just after the blastula stage. On the other hand, *dpp* is started to be

asymmetrically expressed after the trochophore stage (Fig. 2. 4; Iijima et al., 2008). These differences between *dpp* and *nodal* in the timing of asymmetric expression and in the developmental stages when the signal inhibitors are effective suggest that, although the phenotypes are similar, the mechanisms that produced these non-coiled shells are different. That is, the nodal phenotype is likely a result of a loss of the body handedness (Grande and Patel, 2009), while the *dpp* phenotype is likely related to a loss of chirality only in the shell gland and the mantle. The sequence of events also suggests that *dpp* is downstream of *nodal* in the gene regulatory cascade of pulmonate snails.

The *dpp* gene is the invertebrate homolog of bone morphogenetic proteins BMP2 and 4, that are associated with bone formation in vertebrates. I have shown that *dpp* could be one of the essential growth factors in shell formation and shell coiling in gastropods. Although some mathematical models of coiled-shell shapes have been proposed (Raup, 1966; Okamoto, 1988; Ackerly, 1989; Savazzi, 1990; Stone, 1995; Rice, 1998), their biological background has been unclear. In order to understand the relation between the mathematical models and biological realities, more investigations need to be done on the causal relationship between the *dpp* gene and the shell formation, including gene-specific functional analyses such as knockout, knockdown and over-expression of *dpp*.

Chapter Ⅲ

Left-right Asymmetric Expression of *dpp* in the Mantle of Gastropods Correlates with Asymmetric Shell Coiling

3. 1 Introduction

Gastropoda is arguably the most diverse molluscan group. Its members have adapted to various marine and terrestrial ecological niches. One of their distinguishing features is the presence of an external shell in most species. Typologically, the shells can be classified into two groups, coiled and non-coiled (Figure 3. 1). Such a general grouping, however, is highly arbitrary because both groups are likely to be non-monophyletic. Recent phylogenetic and paleontological studies suggest the possibility that shell coiling evolved at the base of the Gastropoda lineage, and that secondary losses of shell coiling occurred several times in various lineages. (Figure 3. 1) (Ponder and Lindberg, 1997; Aktipis et al., 2008). However, although the possible evolutionary path of shell coiling can be inferred from phylogenetic studies, the mechanistic explanation of the morphological changes is not yet understood.

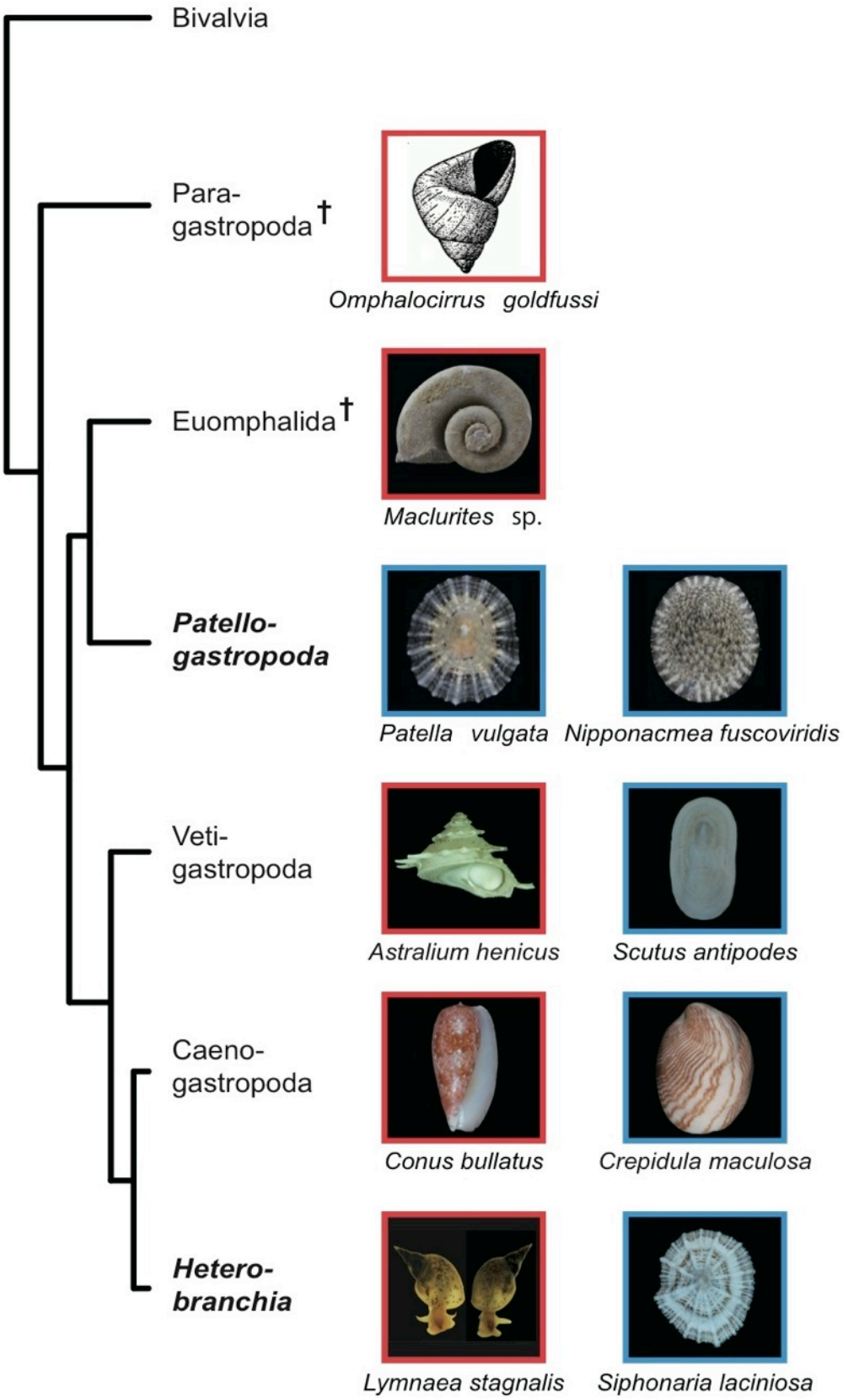

Figure 3. 1 Phylogeny of the Gastropoda and major shell shapes in each group. The phylogeny is based on the studies of Ponder *et al*. (1997) and Aktipis *et al*. (2008). Red boxes indicate coiled shell and blue boxes indicate non-coiled shell. Dagger symbols indicate extinct taxa. Illustration of Paragastropoda is from Knight *et al*. (1960).

To understand the origin of such morphological diversity, we need to look at the developmental mechanisms of the shells. The developmental process of gastropod shells has already been described (Meshcheryakov, 1990; Moril, 1982). The shell gland is formed by the invagination of ectodermal cells at the early trochophore stage (Meshcheryakov, 1990). In the trochophore, shell-secreting cells in the shell gland start to form the initial shell. The mantle tissue begins to develop at the veliger stage, and takes over the role of shell secretion for most of the organism's life (Moril, 1982). Thus, the shell gland is important in early shell formation when the initial trigger and early processes of shell formation occur. Meanwhile, the mantle is involved in shell growth during and after the veliger stage. Accordingly, some previous studies of shell development have focused on these two 'tissues'.

Despite existence of some studies on gastropod shell formation, molecular embryological insight into shell development remains meager. Nederbragt *et al*. (2002) and Iijima *et al*. (2008) reported that the *decapentaplegic* (*dpp*) gene is expressed around the shell gland, suggesting involvement of *dpp* in shell formation. These studies were not conclusive, however, because they studied *dpp* only in the early stages of embryonic development (late gastrula and trochophore stages). To remedy such lack of information, and to conclusively show if *dpp* is involved in shell development in gastropods, we checked the expression patterns of *dpp* in the later developmental stages in three gastropod species: two limpets with a non-coiling shell (*Patella vulgata* and *Nipponacmea fuscoviridis*) and a pond snail with a coiled shell (*Lymnaea stagnalis*). Because *dpp* expression patterns in early developmental stages up to the trochophore were reported in these three species in previous studies (Nederbragt et al., 2002; Iijima et al., 2008; Hashimoto et al., 2012), we confirmed the expression patterns in the veligers and adults. Besides, to reveal the presence of the Dpp gradient in the adult's mantle in coiled shelled snail, I compared expression levels of phosphorylated SMAD1/5/8 (pSMAD1/5/8) that leads to intracellular propagation of the

signal (Figure 3. 2). To understand the involvement of *dpp* expression in shell coiling, we confirmed the *dpp* expression pattern in the trochophore, veliger, and adults of the sinistral mutant of *L. stagnalis*, which have a left-wise coiled shell, and compared the expression patterns with the wild-type (dextral, right-wise coiled shell) strain of the same species (Asami et al., 2008).

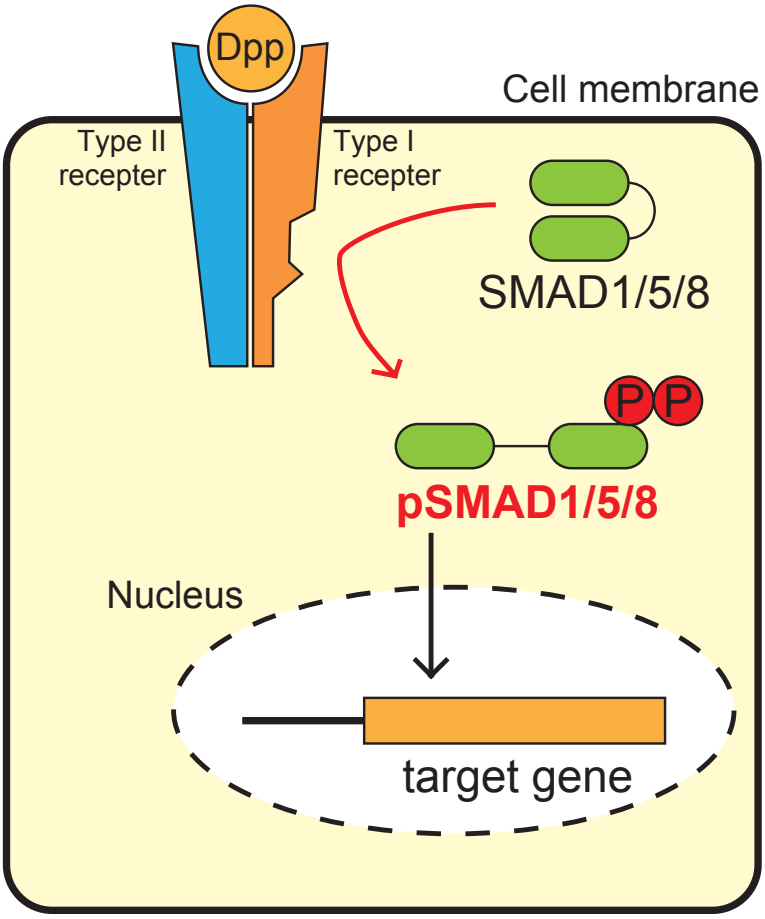

Figure 3. 2 Schematic representation of Dpp signaling pathway. Following Dpp binding to type Ⅰ and Ⅱ receptors, SMAD1/5/8 is phosphorylated by activated type Ⅰ receptor, and phosphorylated SMAD1/5/8 (pSMAD1/5/8) modifies the target gene transcription.

3. 2 Materials and Methods

3. 2. 1 Animal handling

Animal handling followed the guidelines for animal experiments of the University of Tokyo.

3. 2. 2 Animals

Individuals of *P. vulgata* were collected in Shaldon, Devon, UK, and *N. fuscoviridis* in Tateyama, Chiba, Japan. The strains of *L. stagnalis* were reared in tap water in the laboratory. We cultured the dextral strain and sinistral mutant strain of *L. stagnalis* (derived from Shinshu University). Throughout the year, these organisms lay eggs in capsules coated with jelly. Methods of egg collection and culturing followed those in the previous studies on *N. fuscoviridis* and *L. stagnalis* (Kurita et al., 2011; Shimizu et al., 2011).

3. 2. 3 RNA extraction, cDNA synthesis, and gene cloning

We used the mantle tissues of *P. vulgata, N. fuscoviridis,* and *L. stagnalis* for RNA extraction. The mantle tissues were cut off into two parts, left and right. The total RNA was extracted (ISOGEN; Nippon Gene Co. Ltd, Tokyo, Japan), and cDNA synthesis was performed (ReverTra Ace; Toyobo, Osaka, Japan) in accordance with the product protocols. We isolated elongation factor 1 alpha (EF-1α) sequences from *P. vulgata* and *N. fuscoviridis* using degenerate primers designed for Mollusca (Kojima et al., 1997) (Figure 3. 3). We used EF-1α-specific primers for *L. stagnalis* as reported previously (Sarashina et al., 2006). After purification of PCR products using a commercial kit (Gel Extraction Kit; Qiagen Science Inc., Valencia, CA, USA), amplicons were ligated into a vector (pGEM-T Easy Vector; Promega Corp., Madison, WI, USA) using a DNA ligation kit (Promega Corp.), and then transformed to DH5α competent cells (Toyobo).

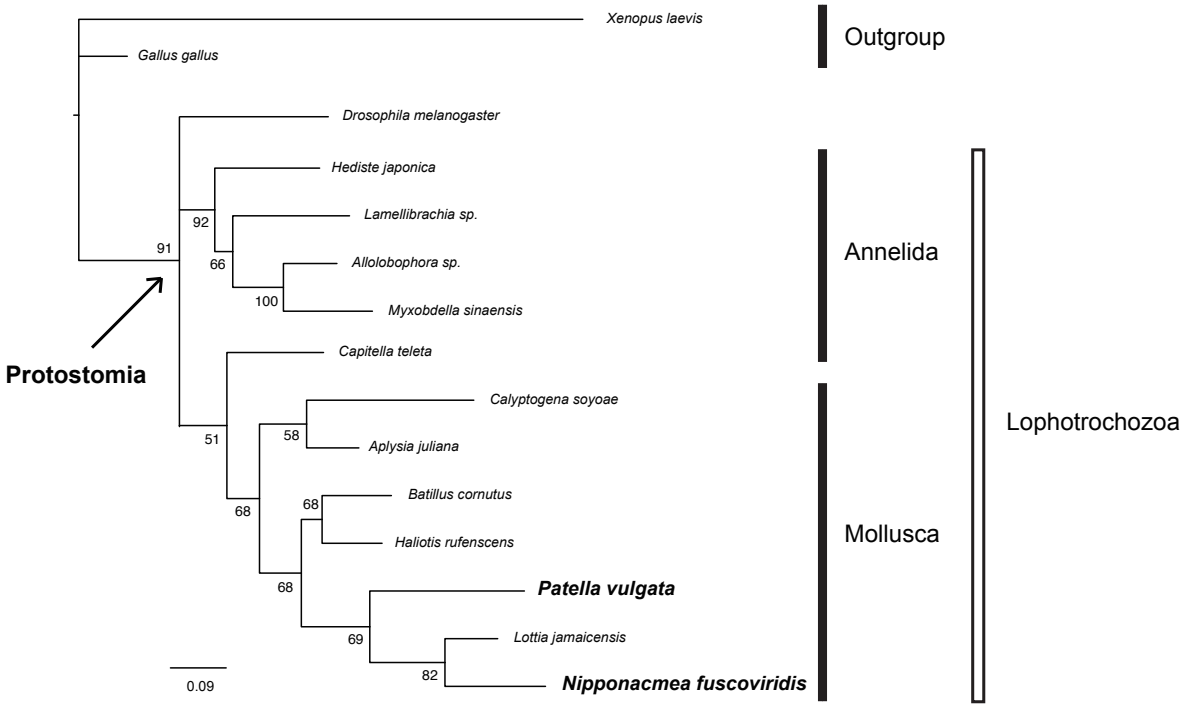

Figure 3. 3 Phylogenetic relationships of elongation factor 1 alpha. Sequence Alignment was performed by MAFFT (http://mafft.cbrc.jp/alignment/server/index.html). Maximum Likelihood (ML) phylogenetic analysis was done using MEGAv5.0 with 100 bootstrap replications. Bootstrap supports below 50% are not shown. *Gallus gallus* (L00677.1), *Xenopus laevis* (NM_001101761.1), *Drosophila melanogaster* (X06869.1), *Hediste japonica* (AB003702), *Lamellibrachia sp.* (AB003721), *Allolobophora sp.* (AB003714), *Myxobdella sinaensis* (AB003716), *Capitella sp.* (AB003706), *Calyptogena soyoae* (AB003719), *Aplysia juliana* (DQ916605.1), *Batillus cornutus* (AB003720), *Haliotis rufenscens* (DQ087488.1), *Lottia jamaicensis* (FJ977772.1).

3. 2. 4 Quantitative reverse transcriptase PCR

Because it is difficult to analyze gene expression patterns in adult specimens using whole-mount *in situ* hybridization, we performed quantitative reverse transcription (qRT)-PCR instead. We designed qRT-PCR primers using the software Primer 3 (Table 3. 1). Relative quantification of total RNA was performed using a commercial solution (SsoFast EvaGreen supermix with low ROX; Bio-Rad Laboratories, Inc., Hercules, CA, USA) and a real-time PCR system (Step One; Applied Biosystems, Foster City, CA, USA). The production of gene-specific products was confirmed by checking their melting curves at the end of qRT-PCR reactions. Data acquisition and analysis were performed (ABI Step One^{TM} software version 2.0; Applied Biosystems). Baselines and thresholds for Ct were set automatically. Quantifications of the target genes were performed by the relative standard curve method. To normalize the quantification of the target gene (*dpp*) expression, we used the housekeeping gene, EF-1α.

Primer name	Sequence
EF-3	GGNCAYMGNGAYTTYRTNAARAAYATGAT
EF-B	CCNCCDATYTTRTANACRTCYTG
PvuEF1a_F1	GTTATCCCCATGGAAACCAG
PvuEF1a_R1	CACGCTCTCTTGGCTTACAC
NfuEF1a_F1	GGTACATCACAGGCCGATTGTG
NfuEF1a_R1	GTCAAATCTGGCCTCGGAGTAG
LstEF1a_F1	TGATCACTGGCACATCACAG
LstEF1a_R1	TCACTGTATGGTGGTGAGGT
Pvudpp_F1	CCATCAGGAATGGTGGAAAC
Pvudpp_R1	CCCGAGTTCATCAGTCCCTA
Nfudpp_F1	TTCCTCTTGGGAGTCGTTTG
Nfudpp_R1	GAATGGGTCTTTGGATTTGC
Lstdpp_F1	CTGAACAAGACACGCCTCAA
Lstdpp_R1	AGTTTTGTTCCATCGCGTTC

Table 3. 1 Sequences of primers used in gene cloning and qRT-PCR.

3. 2. 5 Whole-mount in situ hybridization

We performed *in situ* hybridization as described previously for amphioxus (Yu and Holland, 2009), except for the following changes in the conditions to make it suitable for molluscan embryos. We fixed the *L. stagnalis* embryos with 4% paraformaldehyde in MTSTr (50 mmol/l PIPES-KOH pH 6.9, 25 mmol/l EGTA, 150 mmol/l KCl, 25 mmol/l $MgCl_2$, and 0.1% Triton X-100) (Kuroda et al., 2009). For the other limpet, *P. vulgata,* embryos were fixed with MEMPFA-T (0.1 mol/l MOPS pH 7.4, 2 mmol/l EGTA, 1 mmol/l $MgSO_4$, 4% paraformaldehyde, and 0.1% Tween 20) (Nederbragt et al., 2002) overnight at 4°C.

3. 2. 6 Western blotting

Proteins in the mantle tissues were extracted (ISOGEN; Nippon Gene, Tokyo, Japan) in accordance with the manufacturer's protocol, and were dissolved afterwards in buffer (NuPAGE LDS Sample Buffer; Life Technologies, Corp., Carlsbad, CA, USA). We carried out electrophoresis using 20 μg protein samples on pre-cast polyacrylamide gels with a linear gradient of 4 to 20% (Bio-Rad, Laboratories, Inc., Hercules, CA, USA), and transferred the separated proteins to nitrocellulose membranes. Blocking was performed overnight using 3% BSA in Tris-buffered saline with Tween (TBS-T: 25 mmol/l Tris HCl pH 7.4, 137 mmol/l NaCl, 2.7 mmol/l KCl, and 0.1% Tween-20) at 4°C. Immunodetection was performed using phosphorylated SMAD1/5/8 polyclonal antibody (#9516; Cell Signaling Technology, Danvers, MA, USA) and SMAD1/5/8 polyclonal antibody (sc-6031-R; Santa Cruz Biotechnology, Santa Cruz, CA, USA) at 1:1000 dilution in a commercial solution (Can Get Signal solution 1; Toyobo Co. Ltd, Osaka, Japan). After overnight incubation with the primary antibody at 4°C, the membrane was washed three times in TBS-T, and incubated overnight at 4°C with horseradish peroxidase (HRP)-labeled anti-rabbit antibodies (Thermo Fisher Scientific Inc., Rockford, IL, USA) that were diluted 1:2000 in a commercial solution

(Can Get Signal solution 2; Toyobo,). After washing the membrane three times in TBS-T, it was incubated with a western blotting detection reagent (ECL Prime; GE Healthcare Life Sciences, Little Chalfont, Buckinghamshire UK). The enhanced chemiluminescence signals were detected with a lumino image analyzer (LAS-1000 Plus; Fuji Film, Japan). We measured these signals using ImageJ software (version 1.46.).

3. 2. 7 Statistical analysis

The Wilcoxon–Mann–Whitney test was performed using the statistical software R (version 2.7.1) to evaluate the significant differences in expression levels between the left and right parts of the mantle tissue. $P<0.05$ was considered significant.

3. 3 Results

In the trochophore of the sinistral mutants of *L. stagnalis*, *dpp* is expressed in the left half of the shell gland, mirroring the pattern of the dextral strain, which shows expression of *dpp* only in the right half of the shell (Figure 3. 4A,E). Such asymmetrical expression patterns were seen in the veliger stage also: *dpp* is expressed in the mantle edge as a small spot in the right side only or the left side only in *L. stagnalis* (dextral strain, Figure 3. 4B-D; sinistral strain, F-H). By contrast, *dpp* shows a symmetrical expression pattern in the limpet *P. vulgata*, with *dpp* being expressed circularly around the shell gland at the late trochophore stage (Figure 3. 4I) (Nederbragt et al., 2002). In the early veliger stage, *dpp* ceases to be expressed in the shell field and is expressed in the operculum gland (Figure 3. 4) (Hashimoto et al., 2012). However, *dpp* shows symmetric expression in the mantle edge again at the mid-veliger stage (Figure 3. 4J and K).

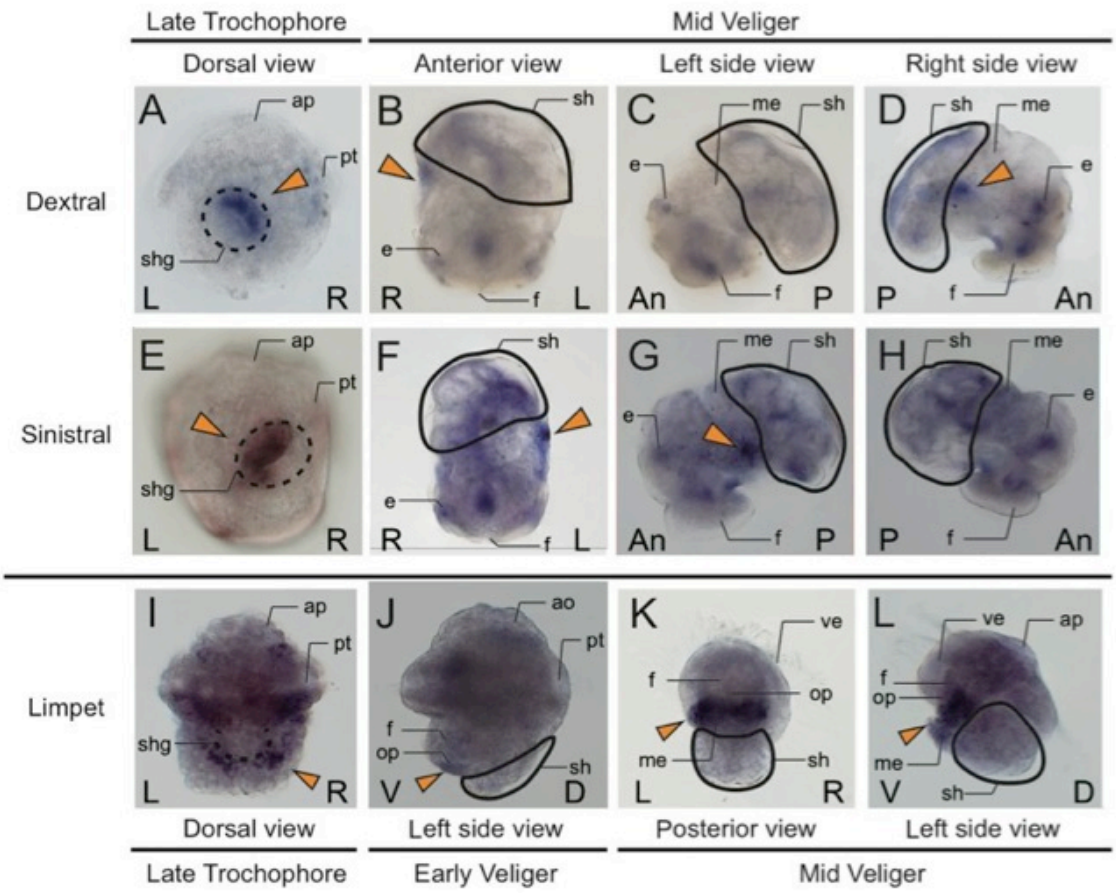

Figure 3. 4 Expression patterns of *dpp* in the trochophore and veliger stages. Expression patterns of *dpp* in **(A, E, I)** the trochophore and **(B–D, F-H, J-L)** veliger stages of the pond snail *Lymnaea stagnalis*, which has a coiled shell (**(A-D)** dextral strain; **(E-H)** sinistral strain) and **(I-L)** the limpet *Patella vulgata*. **(A**, **E**, **I)** Shell gland (dorsal) view; **(B**, **F)** anterior view; **(C**, **G**, **J**, **K)** left side view; **(D**, **H)** right side view; **(K)** posterior view. **(A**, **E**, **I)** Broken black lines indicate the shell gland, and arrowheads indicate the *dpp* expression. **(A-D**, **F-H**, **J-K)** Black lines indicate the shell. **(A–H)** Expression of *dpp* is asymmetric in the shell gland or mantle edge in late trochophore and mid-veliger sages. **(I**, **K**, **L)** Expression of *dpp* is symmetric in late trochophore and mid-veliger stages. **(J)** *dpp* is expressed in the operculum gland. An, anterior; ap, apical plate; d, dorsal; e, eye; f, foot; L, left; m, mouth; me, mantle edge; op, operculum; P, posterior; Pt, prototroch; R, right; sh, shell; shg, shell gland opening; V, ventral; ve, velum.

We then compared the *dpp* expression levels between left and right sides of the mantle edges using qRT-PCR analysis in the three gastropod species. We again found different expression patterns between the coiled and non-coiled shell of the gastropods, consistent with the gene expression patterns described above. In the two limpets *P. vulgata* and *N. fuscoviridis*, whose shells are non-coiled, there was no difference in the *dpp* expression levels between tissue samples taken from the left and the right sides of their mantle edge (Figure 3. 5). By contrast, there was asymmetric *dpp* expression between the left and right sides was seen in the coiled shell *L. stagnalis*; *dpp* expression is higher in the right side of the mantle edge of the wild-type dextral line individuals, and higher in the left side mantle edge in the sinistral mutant individuals (Figure 3. 5).

To confirm the presence of the Dpp gradient in the growing mantle tissues, we compared expression levels of phosphorylated SMAD1/5/8 (pSMAD1/5/8) in the mantle edges using western blotting. In the non-coiled limpet *P. vulgata*, there was no significant difference in pSMAD1/5/8 expression between left and the right sides of the mantle edge (Figure 3. 6), whereas there was asymmetric expression of pSMAD1/5/8 in the coiled shelled snail *L. stagnalis* (Figure 3. 6). These results indicate that a Dpp signal gradient indeed exists in the mantle edge of the coiled-shell snail, whereas Dpp signals are distributed symmetrically in the non-coiled-shell limpet.

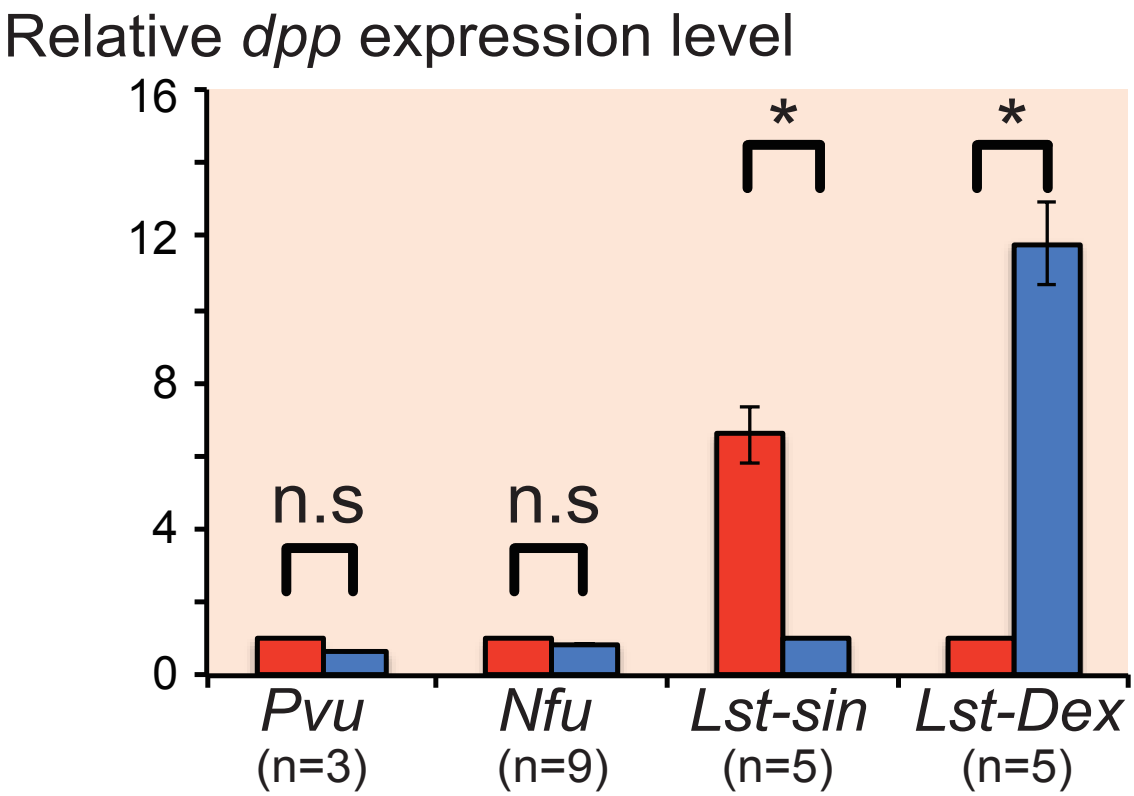

Figure 3. 5 Expression levels of *dpp* transcripts in adult mantle edge tissue. Comparison of the levels of *dpp* transcripts between the left and right sides of the mantle tissue by quantitative reverse transcription (RT)-PCR analysis using EF-1α transcripts as reference. In the non-coiled shelled limpets, *Patella vulgata* and *Nipponacmea fuscoviridis*, *dpp* expression levels were not different between left and right sides of mantle tissues. By contrast, in the coiled-shell snail *Lymnaea stagnalis* (dextral and sinistral), *dpp* expression levels were significantly different (asymmetric) (Wilcoxon–Mann–Whitney test; $P<0.05$). Gene expression levels were standardized by dividing the values by those of the left side (*P. vulgate*, *N. fuscoviridis,* and the dextral strain of *L. stagnalis*), or by those of the right side (sinistral strain of *L. stagnalis*). Error bars represent standard deviations.

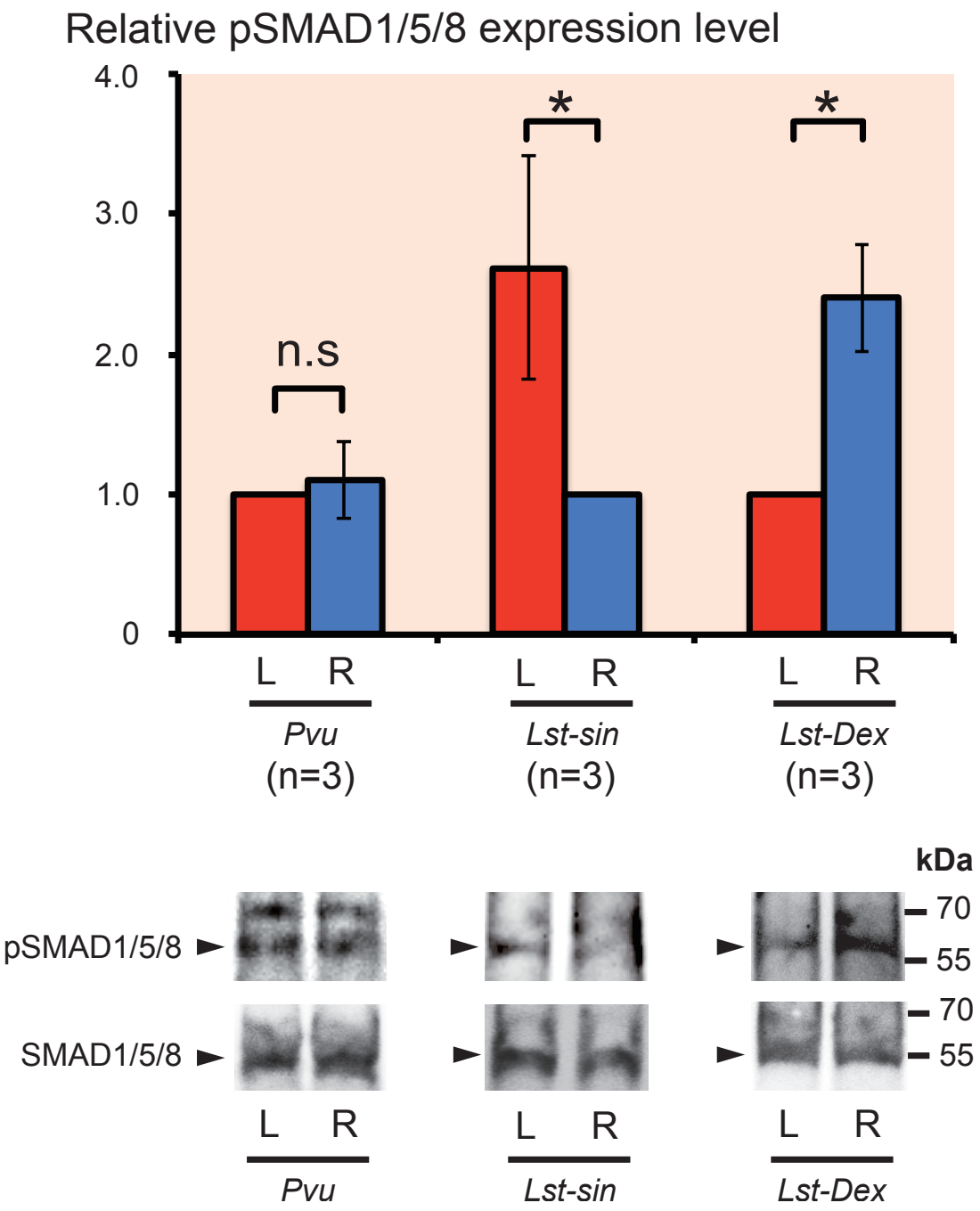

Figure 3. 6 Expression levels of pSMAD1/5/8 in adult mantle edge tissues. Comparisons of the levels of pSMAD1/5/8 between left and right sides of the mantle tissue by western blotting. In the non-coiled shelled limpet *Patella vulgata,* pSMAD1/5/8 expression levels were not different between left and right sides of the mantle edges. By contrast, in the coiled-shell snail *Lymnaea stagnalis* (dextral and sinistral), pSMAD1/5/8 expression levels were significantly different (asymmetric) (paired t-test; $P<0.05$). Expression levels were standardized by dividing the values by those of the left side (*P. vulgata*, *Nipponacmea fuscoviridis,* and the dextral strain of *L. stagnalis*), or by those of the right side (sinistral strain of *L. stagnalis*). Error bars represent standard deviations.

3. 4. Discussion

In the field of theoretical morphology of biological shapes, coiling shells have drawn considerable interest for many years. Rice (1998) provided a theoretical model based on the idea that the animal must keep a constant gradient of shell growth rate between the outer and inner edge (the gradient) to produce a coiling shell. This idea has been incorporated in many recent models for shell growth (for example, Hammer et al., 2005; Urdy et al., 2010). By contrast, the molecular basis of shell coiling is poorly understood to date. Probably it is interested that a morphogen-like gradient substance exists, but no candidate for such a concentration gradient has yet been identified. Our results suggest that the left–right gradient of the Dpp protein (caused by a left–right asymmetric expression of the *dpp* gene) could be the most likely candidate for the gradient in shell coiling, as discussed for some previous mathematical models (Rice, 1998; Urdy et al., 2010; Hammer et al., 2005).

In this study, we found that in the coiled-shell snail *L. stagnalis*, *dpp* is expressed in the local spot of the left or right side mantle edge that corresponds with the shell-coiling direction at the veliger stage, and continues being expressed asymmetrically until the adult stage (Figure 3. 4A-H; Figure 3. 5). By contrast, in the limpets, *dpp* continues to be expressed symmetrically from the late trochophore stage to the adult stage (Figure 3. 4I, K, L; Figure 3. 5). Furthermore, we found by western blotting using anti-phosphorylated SMAD1/5/8 antibodies that Dpp signals are indeed distributed asymmetrically in the mantle edge in the coiled-shell snail and symmetrically in the non-coiled-shell limpet (Figure 3. 6). In the fruit fly, Dpp works as a morphogen during wing development, spreading through the target point and forming a concentration gradient that provides positional information (Nellen et al., 1996). Rogulja *et al*. (2005) further showed that Dpp triggers cell division, and the division activity correlates positively with the concentration of Dpp gradient. Hashimoto *et al*. (2012) suggested that in gastropods, Dpp might function by triggering the regulation of cell

division in the mantle during shell formation. The cells of the mantle edge secrete shell-matrix proteins, and these proteins are transferred to the outer edge of the shell and mineralized with $CaCO_3$. Therefore, if cells rapidly proliferate, more cells can secrete shell-matrix proteins in any one unit of time. We thus propose that during coiled-shell development, Dpp acts as a trigger for an asymmetric cell proliferation, by producing a concentration gradient in the mantle from one spot of expression, and diffuses to the other side of the mantle (Figure 3. 7A). The Dpp gradient might then cause several different reaction thresholds, which in turn induce different levels of cell proliferation along the aperture (Figure 3. 7B). These different levels of cell division might then cause an asymmetric aperture expansion, causing a non-uniform shell growth (Figure 3. 7C) and resulting in a coiled shell (Figure 3. 7D). Constant asymmetric expression of *dpp,* and thus a constant presence of the gradient until the veliger and adult stage of the snail, ensures the constant coiling during shell growth. Meanwhile, in the non-coiled-shelled limpets, symmetric aperture expansion and shell growth occurs because *dpp* is expressed symmetrically in the shell gland and the mantle edge, causing uniform cell division (Figure 3. 4, Figure 3. 5, Figure 3. 6, Figure 3. 7).

A recent report (Shimizu et al., 2011) of functional analysis of Dpp in *L. stagnalis* supports this hypothetical mechanism of shell coiling. When the embryos were treated with a Dpp signal inhibitor (dorsomorphin) at the trochophore and veliger stages, the juvenile shells showed a cone-like form rather than a normal coiled form (Shimizu et al., 2011). These results indicated that Dpp signals induce differences in shell growth rates around the aperture by their gradient. The molecular results presented here support this mathematical models for shell growth (Rice, 1998; Urdy et al., 2010; Hammer et al., 2005).

The molecular developmental insights into shell coiling reported here also explain how shell coiling was lost several times during the evolution of gastropods. Although it is difficult

to infer the ancestral shell shape (coiled or non-coiled shell), previous phylogenetic studies showed that the non-coiled-shelled gastropod Patellogastropoda is placed as the sister group to the rest of extant gastropods (Figure 3. 1; Figure 3. 8). However, considering the fossil record, Paragastropoda that have coiled shells are possibly the most recent common ancestor of gastropods (Ponder and Lindberg, 1997), hence suggesting that the coiled-shell feature is probably synplesiomorphy and the non-coiled shell shape has evolved independently several times in gastropods (Figure 3. 1; Figure 3. 8) (Ponder and Lindberg, 1997; Aktipis et al., 2008). Our current results suggest that the loss of coiling might have happened relatively easily, by losing the asymmetric expression of *dpp* (or its upstream regulators) in the shell gland at the trochophore stage, and leading to symmetric *dpp* expression n the veliger and adult stages. Further investigations are needed to understand the molecular mechanisms of shell formation and evolution, because the process of shell development is very complex. However, the new insight provided by the current study into *dpp* expression patterns in the mantle edge, not only in the early developmental stages but also in later stages, is the key basis for understanding how various shell shapes evolved and are formed in gastropods.

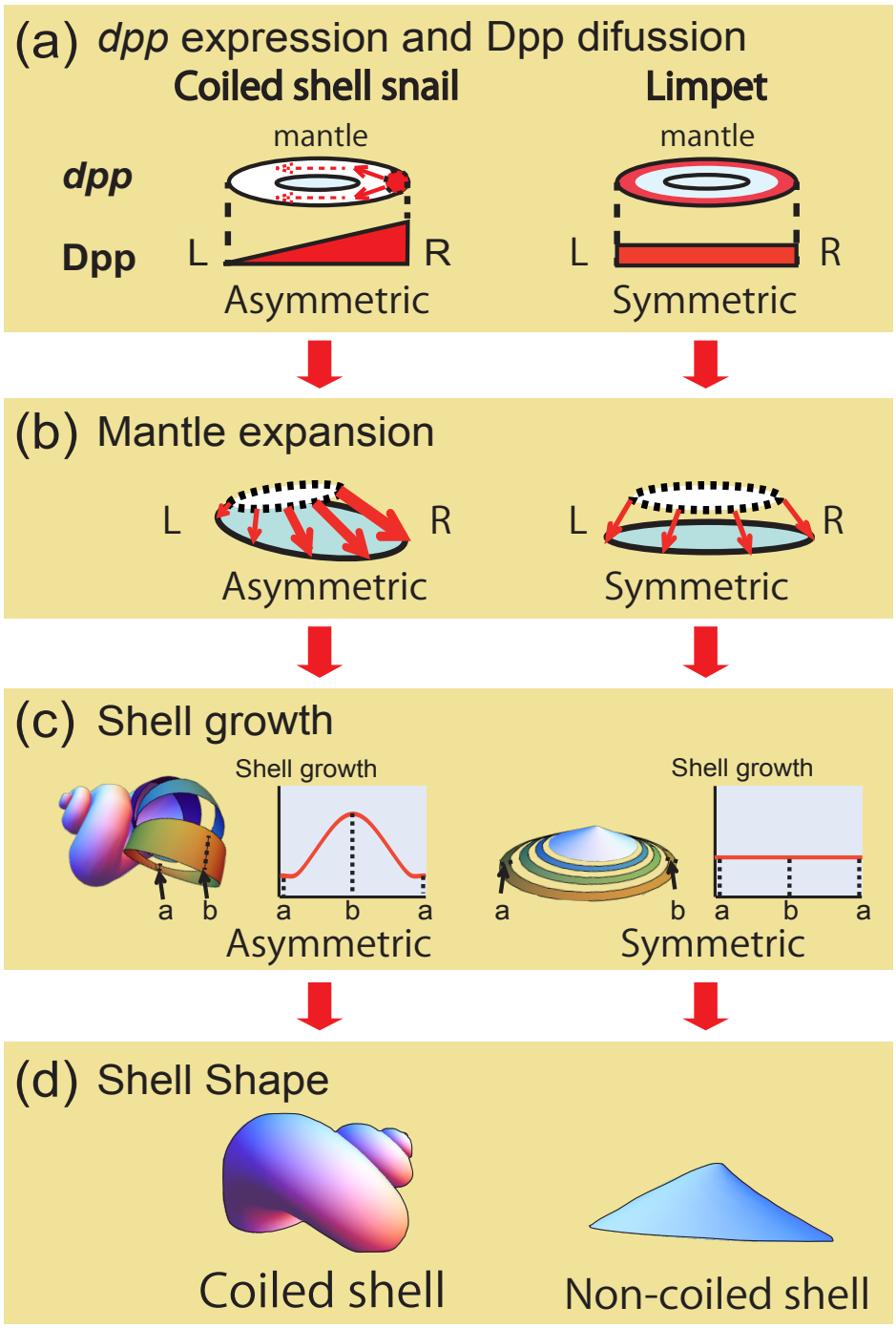

Figure 3. 7 A molecular hypothesis of shell coiling in Gastropoda. (A) In a snail with a coiled shell, *dpp* (red) is expressed asymmetrically in the mantle, and Dpp diffusion causes an asymmetric concentration gradient in the mantle. **(B)** Asymmetric mantle expansion is induced by asymmetric Dpp localization, because Dpp controls cell proliferation in the mantle [8]. **(C, D)** As a result of the asymmetric mantle expansion, non-uniform shell growth occurs, and produces a coiled shell. By contrast, in the limpets, a non-coiled shell is formed because the lack of expression of *dpp* in the mantle results in symmetric mantle expansion and shell growth. L, left; R, right.

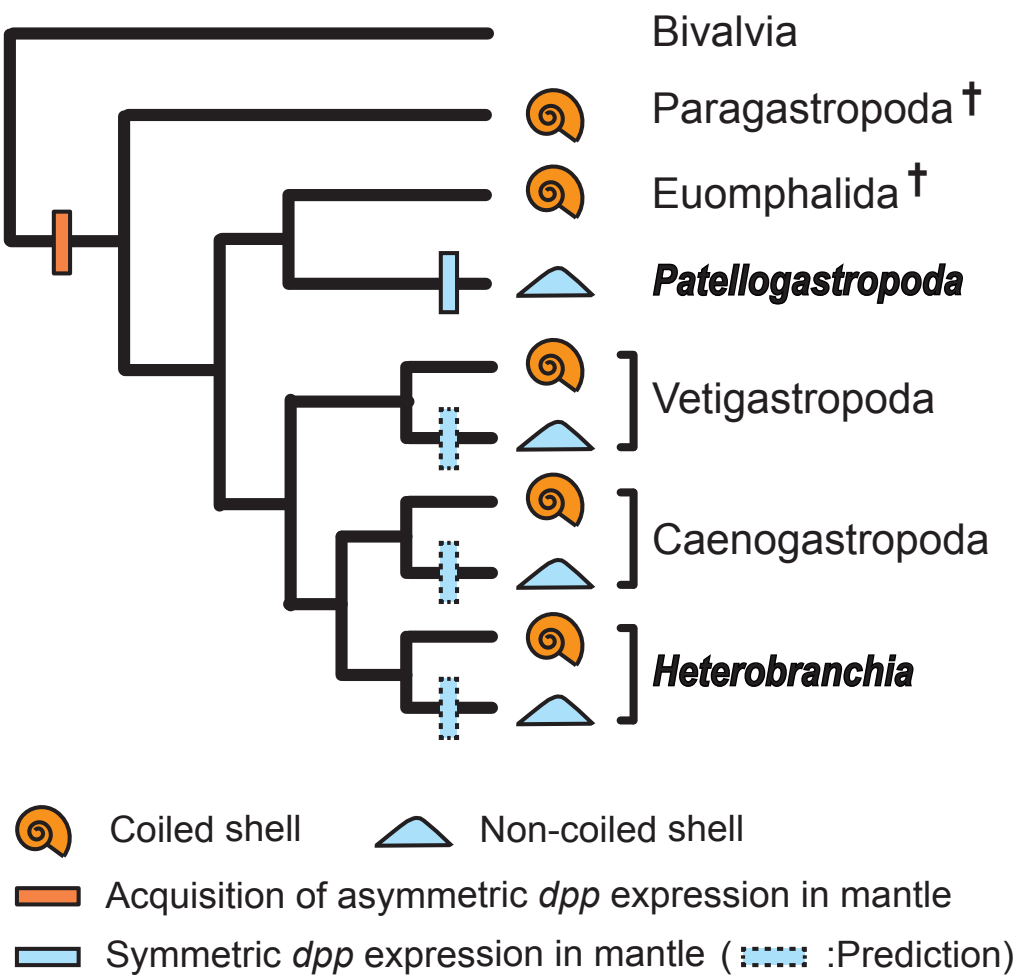

Figure 3. 8 Evolutionary hypothesis of the shell-coiling mechanism in Gastropoda. The most recent common ancestor of Gastropoda acquired the asymmetric *dpp* expression pathway in the mantle at one stage (orange line). Later, the Patellogastropoda lost this pathway and the non-coiled shell shape evolved in this group (blue line). Moreover, other species with non-coiled shells in Vetigastropoda, Caenogastropoda or Heterobranchia most likely evolved like Patellogastropoda (broken blue lines).

In this study, we found that continuous expression of *dpp* in the mantle edge until the adult stage might explain the mechanism of these two variations in gastropod shell shapes, that is, the coiled and the non-coiled shapes. However, because in this study we used only patellogastropod species (*P. vulgata* and *N. fuscoviridis*), further molecular studies of the species other than those of the Patellogastropoda, such as those from other non-coiled-shell snails are needed in order to be able to infer a decisive conclusion about the evolution of shell-coiling loss in gastropods (Figure 3. 1).

3. 5. Conclusion

We found crucial differences in *dpp* expression patterns between non-coiled-shell limpets and coiled-shell gastropods with a dextral or a sinistral shell, not only in the early developmental stages but also in the late stages. By cross-referencing with previous functional analyses of *dpp* in gastropods and other animals (Hashimoto et al., 2012; Shimizu et al., 2011; Nellen et al., 1996; Rogulja et al., 2005) and previous mathematical models (Rice, 1998; Urdy et al., 2010; Hammer et al., 2005), we suggest a hypothesis of shell coiling based on the presence of a Dpp gradient. We hypothesize that Dpp induces mantle expansion, corresponding to the pattern of the concentration gradient of the Dpp morphogen (Figure 3. 7). This hypothesis provides plausible biological grounds for previously published mathematical models of shell formation (Rice, 1998; Urdy et al., 2010; Hammer et al., 2005). Our results also suggest a molecular explanation for the shell-coiling mechanism in gastropods, and thus provide robust preliminary information to answer the question about how the diverse gastropod shell shapes evolved.

Chapter Ⅳ

Anterior-posterior Asymmetric Dpp Expression and Evolution of the Coiled Shelled Cephalopods

本章については、5年以内に 雑誌等で刊行予定のため、非公開。

本章については、5 年以内に 雑誌等で刊行予定のため、非公開。

本章については、5 年以内に 雑誌等で刊行予定のため、非公開。

本章については、5 年以内に 雑誌等で刊行予定のため、非公開。

本章については、5 年以内に 雑誌等で刊行予定のため、非公開。

本章については、5 年以内に 雑誌等で刊行予定のため、非公開。

本章については、5 年以内に 雑誌等で刊行予定のため、非公開。

本章については、5 年以内に 雑誌等で刊行予定のため、非公開。

本章については、5 年以内に 雑誌等で刊行予定のため、非公開。

本章については、5 年以内に 雑誌等で刊行予定のため、非公開。

本章については、5 年以内に 雑誌等で刊行予定のため、非公開。

本章については、5 年以内に 雑誌等で刊行予定のため、非公開。

本章については、5 年以内に 雑誌等で刊行予定のため、非公開。

本章については、5 年以内に 雑誌等で刊行予定のため、非公開。

本章については、5 年以内に 雑誌等で刊行予定のため、非公開。

Chapter Ⅴ

A Novel Role of RA Signaling Pathway in Molluscan Shell Formation

本章については、5年以内に 雑誌等で刊行予定のため、非公開。

本章については、5 年以内に 雑誌等で刊行予定のため、非公開。

本章については、5 年以内に 雑誌等で刊行予定のため、非公開。

本章については、5 年以内に 雑誌等で刊行予定のため、非公開。

本章については、5 年以内に 雑誌等で刊行予定のため、非公開。

本章については、5 年以内に 雑誌等で刊行予定のため、非公開。

本章については、5 年以内に 雑誌等で刊行予定のため、非公開。

本章については、5 年以内に 雑誌等で刊行予定のため、非公開。

本章については、5 年以内に 雑誌等で刊行予定のため、非公開。

本章については、5 年以内に 雑誌等で刊行予定のため、非公開。

本章については、5 年以内に 雑誌等で刊行予定のため、非公開。

本章については、5 年以内に 雑誌等で刊行予定のため、非公開。

本章については、5 年以内に 雑誌等で刊行予定のため、非公開。

本章については、5 年以内に 雑誌等で刊行予定のため、非公開。

本章については、5 年以内に 雑誌等で刊行予定のため、非公開。

本章については、5 年以内に 雑誌等で刊行予定のため、非公開。

本章については、5 年以内に 雑誌等で刊行予定のため、非公開。

本章については、5 年以内に 雑誌等で刊行予定のため、非公開。

本章については、5 年以内に 雑誌等で刊行予定のため、非公開。

本章については、5 年以内に 雑誌等で刊行予定のため、非公開。

本章については、5 年以内に 雑誌等で刊行予定のため、非公開。

Chapter Ⅵ

An *in-silico* Genomic Survey to Annotate Genes Coding for Early Development-relevant Signaling Molecules, TGF-β Superfamily, in the Pearl Oyster *Pinctada fucata*

6. 1 Introduction

Current progress in molecular developmental biology has brought a deep understanding of the molecular underpinnings of animal body morphogenesis. For instance, it has known that seven of about 20 signaling pathways controlling cellular interactions and differentiations are involved in the morphogenetic processes during embryonic development in metazoans (Barolo & Posakony, 2002; Pires-da Silva & Sommer, 2003; Gazave et al., 2009). The full genome sequence of target animal is powerful information to understand their morphogenesis. Recently, the full nuclear genome sequence of the Japanese pearl oyster *Pinctada fucata* was determined (Takeuchi et al., 2012), and EST libraries from an adult (Kinoshita et al., 2011) and various developmental stages were prepared. These reports of genomic tools provide the important information to understand the developmental system in Mollusca.

Signal molecules have a complex interaction among other kind of signal molecules and the morphogenesis is correctly regulated by these interactions. In previous studies, it has reported that the shell formation is correlated with Dpp signal that is one of the signal molecules in gastropods and bivalves (Shimizu et al. 2011 and 2013; Hashimoto et al. 2012). However, *dpp* is nothing more than one gene belonging to the TGF-β superfamily that is one of the signal molecules families. In order to understand the molluscan shell development, it is necessary to investigate the function of other TGF-β superfamily genes.

As one of the initial steps of providing basic information needed to establish the Japanese

pearl oyster as a model system, in this paper, I focused on the TGF-β superfamily genes involved in morphogenesis such as shell development. Signaling molecules play important roles in many morphogenetic events during various stages of development such as axis formation, muscle differentiation, and nervous system development. They work by diffusing out from a signaling center, producing a concentration gradient. These molecules, also known as morphogens, bind to receptors located on surrounding cells, prompting receptive cells to produce specific responses depending on the concentration of the signaling molecules reached them. This study found most members of the TGF-β superfamily genes that are reported to be present in the protostomes. I then discussed the implication of the findings for the interpretation of the evolution of protostomes' signaling molecule genes involved in their early development.

6. 2 Materials and Methods

6. 2. 1 Gene model searches and confirmations

I conducted two different methods to identify *Pinctada fucata* gene homologs. For the first method, I obtained amino acid sequences of the genes of interest from other organisms from GenBank. *P. fucata* gene search was conducted by using the retrieved sequences as TBLASTN and BLASTP queries on the *P. fucata* gene models version 1.1 and genome assembly version 1.0, which was conducted using the available Genome Browser (http://marinegenomics.oist.jp/pinctada_fucata). For the second method, I used the "Pfam domain search" function available on the *P. fucata* Genome Browser.

The amino acid sequences of the obtained gene models from both identification methods were then subjected to TBLASTN and BLASTP against NCBI non-redundant (nr) database for identification confirmation. I also conducted TBLASTN and BLASTP searches against the *P. fucata* transcriptome EST database, which is available at the Genome Browser (Takeuchi et al., 2012), to obtain additional confirmation for the gene models. The EST sequence data were obtained through transcriptome sequencing using 454 Next Generation Sequencer, of several embryonic and adult individuals.

To deduce the evolution of the signaling molecule genes in bilaterian animals especially in lophotrochozoans, I did quick surveys on two lophotrochozoans for which annotated draft genomes were available: the gastropod *Lottia gigantea* (http://genome.jgi-psf.org/Lotgi1/Lotgi1.home.html) and the polychaete *Capitella teleta* (http://genome.jgi-psf.org/Capca1/Capca1.home.html).

6. 2. 2 Phylogenetic analyses of signaling molecule-coding genes

For phylogenetic analyses of the signaling molecule genes with multiple paralogous copies, I used sequences of the gene models obtained from the *P. fucata* genome. I used EST sequences when they showed longer conserved domain sequence of the gene than those predicted by the gene models. I then used conserved domain sequences from human (Hs) and fruit fly (Dm) obtained from GenBank. I also obtained homologous sequences from the draft genome of the two lophotrochozoans, the polychaete *Capitella teleta* (Ct) and the limpet *Lottia gigantea* (Lg), by doing TBLASTN and BLASTP to genome sequences using various queries (Table 6. 1). I then predicted their conserved protein domains using SMART, and included the domain sequences in these phylogenetic analyses.

Sequence alignments were conducted using the online version of PROMALS3D program, since this program allows users to input structural constraints for known domains (Pei et al., 2008). Accordingly, I first obtained "core" domain alignments from PROSITE (http://prosite.expasy.org/) and used them as alignment constraints in PROMALS3D. The obtained alignment was then edited manually by using Mesquite v2.75 (Maddison & Maddison, 2011) or MEGA v5.0 (Tamura et al., 2011). Afterwards, I used MEGAv5.0 to search for the best amino acid substitution model of the edited alignments. In most occasions, the top four models suggested were WAG+G, WAG+G+I, JTT+G, and JTT+I+G. Whenever possible, I used the best model suggested, in these subsequent phylogenetic analyses. Maximum Likelihood (ML) phylogenetic analyses were conducted using the online version of RAxML (RAxML Blackbox; Stamatakis et al., 2008; http://phylobench.vital-it.ch/raxml-bb/), with 100 bootstrap replications.

Gene Name	Accession No.	Gene Name	Accession No.
HsBMP2	NP_001191.1	HsBMPR1B	O00238
HsBMP3	NP_001192.2	HsACTR2A	NP-001607.1
HsBMP4	NP_001193.2	HsACTR2B	Q13705
HsBMP5	NP_066551.1	HsBMPR2	Q13873
HsBMP6	NP_001709.1	HsTGFBR2	P37173
HsBMP7	NP_001710.1	DmDpp	NP_477311.1
HsBMP8A	NP_861525.2	DmGbb	NP_477340.1
HsBMP8B	NP_001711.2	DmScw	NP_524863.3
HsBMP9	NP_057288.1	DmMaverick	NP_524626.1
HsBMP10	NP_055297.1	DmMyoglianin	NP_726606.1
HsGDF1	NP_001483.3	DmActivin-b	NP_651942.2
HsGDF3	NP_065685.1	DmAlp	NP_722840
HsGDF5	NP_000548.1	DmSax	AAA18208.1
HsGDF6	NP_001001557.1	DmBabo	NP-477000.1
HsGDF8	NP_005250.1	DmTkv	AAA28996.1
HsGDF11	NP_005802.1	DmPut	AAC41566.1
HsNodal	NP_060525.3	DmWit	NP-524692.3
HsLefty1	NP_066277.1	CtDpp	jgi|Capca1|73817|gw1.16.141.1
HsTGFB1	NP_000651.3	CtBMP3	jgi|Capca1|147335|e_gw1.10.100.1
HsTGFB2	NP_001129071.1	CtGbb	jgi|Capca1|83310|gw1.1723.4.1
HsTGFB3	NP_003230.1	CtBMP9/10	jgi|Capca1|132548|e_gw1.1800.1.1
HsInhibin-bA	NP_002183.1	CtNodal	jgi|Capca1|197270|fgenesh1_pg.C_scaffold_774000001
HsInhibin-bB	NP_002184.2	CtMyostatin	jgi|Capca1|39276|gw1.17.62.1
HsInhibin-bC	NP_005529.1	LgDpp	jgi|Lotgi1|205842|estExt_fgenesh2_pm.C_sca_70027
HsInhibin-bE	NP_113667.1	LgGbb	jgi|Lotgi1|195882|estExt_Genewise1.C_sca_700162
HsALK1	P37023	LgBMP9/10	jgi|Lotgi1|111943|e_gw1.14.89.1
HsALK2	Q04771	LgNodal	ACB42423.1
HsALK3	P36894	LgMyostatin	jgi|Lotgi1|82990|gw1.97.130.1
HsALK4	P36896	LgActivin	jgi|Lotgi1|151945|fgenesh2_pg.C_sca_1000083
HsALK5	P36897		

Table 6. 1 Accession numbers used in phylogenetic analysis.

6. 2. 3 Protein domain re-prediction using SMART for signaling molecule genes

Although the Genome Browser provided a domain prediction for all of its gene models, for further confirmation, I re-predicted the domain structure using the online version of the protein domain annotation software, SMART (Letunic et al, 2012; Schultz et al., 1998; http://smart.embl-heidelberg.de/). I based the diagrams of the domain structures of the signaling on SMART results. In the figure of this paper, I only provided the diagrams of this gene models and not of the EST sequences.

6. 3 Results and Discussion

6. 3. 1 TGFβ superfamily in bivalve Pinctada fucata

TGFβ superfamily consists of two subfamilies, the BMP and the Activin/ TGFβ subfamilies. A typical TGFβ ligand has two conserved domains, the TGFβ propeptide and TGFβ like domains (Fig. 6. 1). Previous molluscan studies have identified three TGFβ ligand-coding genes (Nederbragt et al., 2002; Grande and Patel, 2009; Kin et al., 2009). However, those previous studies suffered from the lack of genomic data. I thus conducted a genomic survey of TGFβ superfamily ligands in the *P. fucata* to look for their presence in the genome. I annotated five gene models as homologs of the BMP subfamily ligands (*dpp-bmp2/4, bmp3, gbb-bmp5-8, bmp9/10*, and *nodal*), an Activin/TGFβ subfamily ligand (*myostatin*), and *maverick*. The homology of each copy was checked by TBLASTN, BLASTP, and phylogenetic analysis. The resulting phylogenetic tree (Fig. 6. 2) confidently placed each copy with its tentative homologous genes from other bilaterians, with reasonable bootstrap supports.

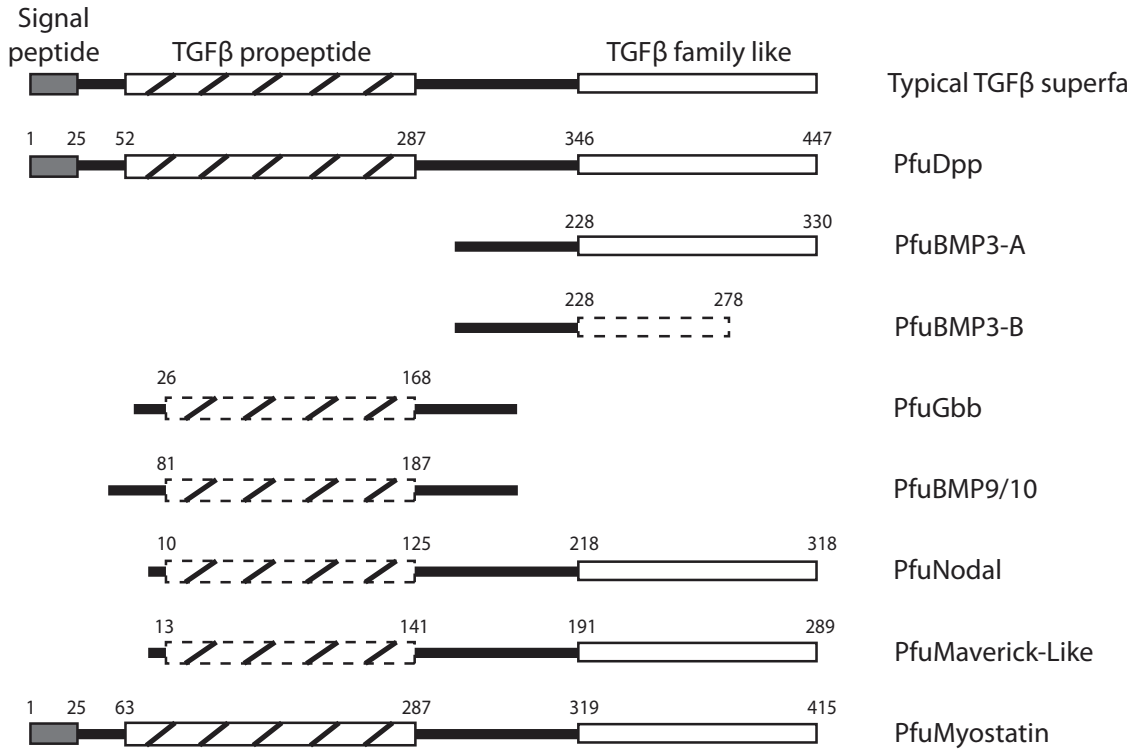

Figure 6. 1 The protein structure of TGFβ superfamily ligands. I identified a complete Pifuc-Dpp sequence with all expected domains present. However, other gene models of TGFβ ligands are most likely partial sequences lacking one or more domains of the signal peptide, the TGFβ propeptide, or the TGFβ family-like. Rectangles with broken lines indicate partial predicted domains.

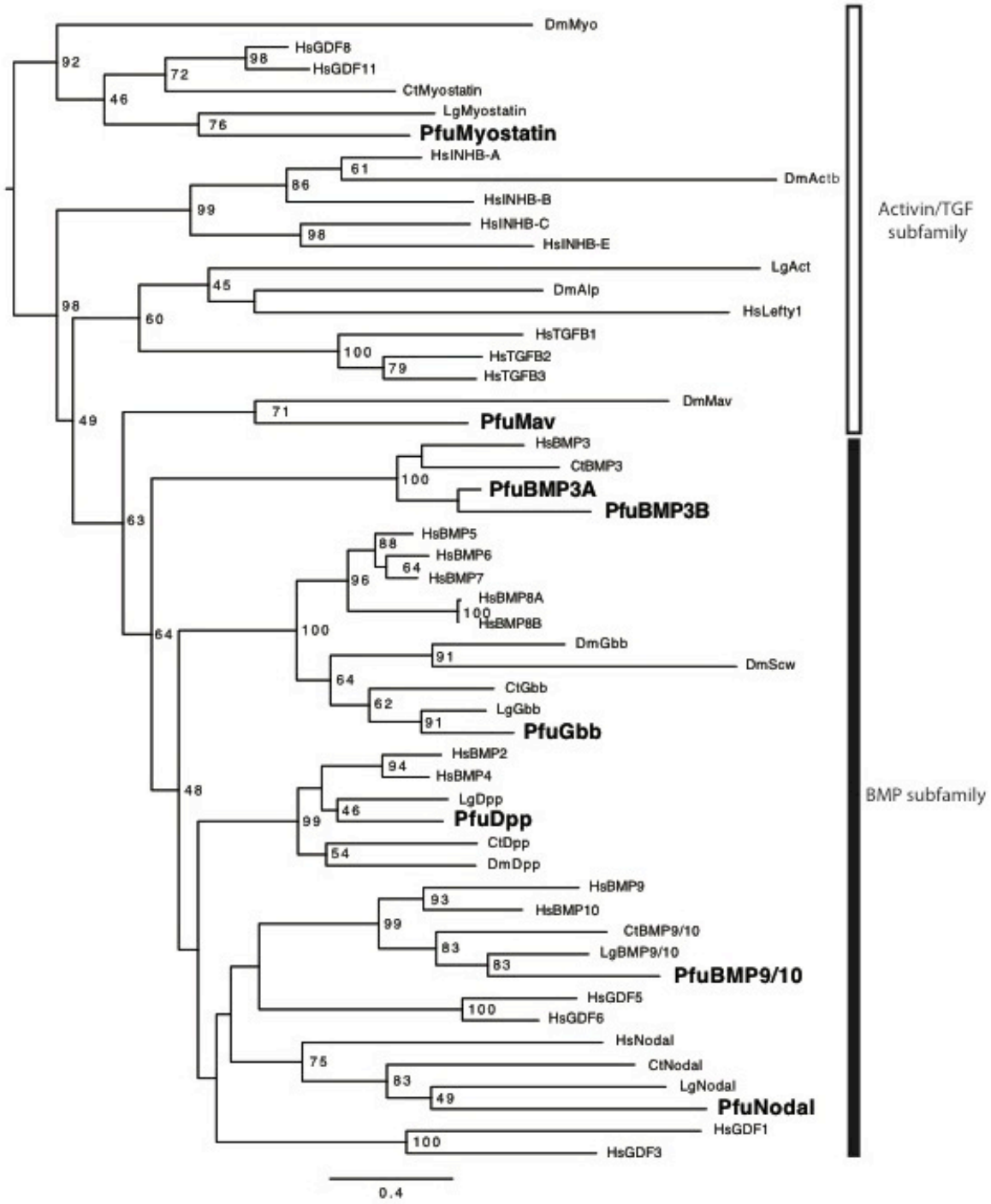

Figure 6. 2 The phylogenetic tree of TGFβ superfamily genes
Phylogenetic tree of TGFβ superfamily ligand genes. I included homologs from fruit fly (Dm), human (Hs), limpet (Lg), and a polychaete (Ct) (Supplementary Table 4). The two subfamilies, i.e. the BMP and Activin/ TGFβ subfamilies, were divided into two monophyletic clades. The eight gene models of *P. fucata* are placed within the respective clades of homologous genes, which is in accordance with the BLAST results. Bootstrap supports below 40% are not shown.

I could not find any gene model or EST for the other three TGFβ family ligands (i.e. *activin*, *tgfβ*, and *lefty*) in the currently available predicted gene models and the transcriptome data. The survey on the genome data of *L. gigantea* and *C. teleta* also failed to find any gene model for *tgfβ* and *lefty*. Previous studies have suggested that the absence of *tgfβ* and *lefty* is probably synapomorphic to protostomes (e.g. Van der Zee et al., 2008).

The genomic survey also failed to identify any gene model for *activin* in *L. gigantea* and *C. teleta*. Although Grande and Patel (2009) have reported the presence of an *activin* homolog in *L. gigantea*, they could not detect its expression in the developing embryo, leaving its function unclear, while its affinity to other *activin* homologs was lowly supported. In the phylogenetic analyses, the reported *Lg activin* grouped with fruitfly's *activin-like protein* with low support (Fig. 6. 2), but not with other *activin*s. I also identified five gene models for TGFβ receptors (*bmp receptor type I*, t*ype II*, *activin receptor type I*, *IB* and *type II*) in the *P. fucata* genome (Table 6. 2, Fig. 6. 3). Since Myostatin and probably other BMP ligands also bind to the Activin receptors (Huminiecki et al., 2009), the presence of the receptors does not necessarily suggest the presence of *activin*. All said, with this current data, I am unable to confidently conclude the presence of *activin* in mollusks, or lophotrochozoans. Therefore, future genomic and molecular analyses will be needed to conclusively show if *activin* is really present or absent in *P. fucata* and other mollusks. However, since the presence of two *activin* homologs has also been reported in the fruitfly (Zhu et al., 2008), I can deduce that the presence of *activin* is probably ancestral to protostomes (Fig. 6. 4).

Family	Category	gene name	gene model number in assembly	gene model ID	BLAST best hit (accession + species)
TGFβ	Ligand	Dpp-BMP2/4	1	pfu_aug1.0_790.1_51081.t1	BAD16731.1, [*Pinctada fucata*]
		BMP3	2	pfu_aug1.0_43625.1_63151.t1	ACF93445.1, [*Branchiostoma japonicum*]
				pfu_aug1.0_102538.1_06302	XP_001494823.2, [*Equus caballus*]
		Gbb-BMP5-8	1	pfu_aug1.0_23580.1_26106	XP_002407531.1, [*Ixodes scapularis*]
		BMP9/10	1	pfu_aug1.0_2637.1_30198	CAD67715.1, [*Crassostrea gigas*]
		Nodal	1	pfu_aug1.0_447.1_29262	ACB42422.1, [*Biomphalaria glabrata*]
		Myostatin	1	pfu_aug1.0_156.1_22035	ABJ09581.2, [*Chlamys farreri*]
		Marverick-like	1	pfu_aug1.0_6051.1_16824	CAD67714.1, [*Crassostrea gigas*]
TGFβ	Receptor	BMPR1	1	pfu_aug1.0_257.1_50753	CAE11917.1, [*Crassostrea gigas*]
		BMPR2	2	pfu_aug1.0_14312.1_32434	XP_001184902.1, [*Strongylocentrotus purpuratus*]
				pfu_aug1.0_27640.1_04591	XP_001184902.1, [*Strongylocentrotus purpuratus*]
		ACVR1	2	pfu_aug1.0_40446.1_70	ADD80738.1, [*Pinctada fucata*]
				pfu_aug1.0_38196.1_0503	ADD80738.1, [*Pinctada fucata*]
		ACVR1B	1	pfu_aug1.0_11.1_50544	CAD20573.1, [*Crassostrea gigas*]
		ACVR2	1	pfu_aug1.0_3667.1_16148	CAR92545.1, [*Crassostrea gigas*]

Table 6. 2 Axial patterning related signaling molecules and their receptors

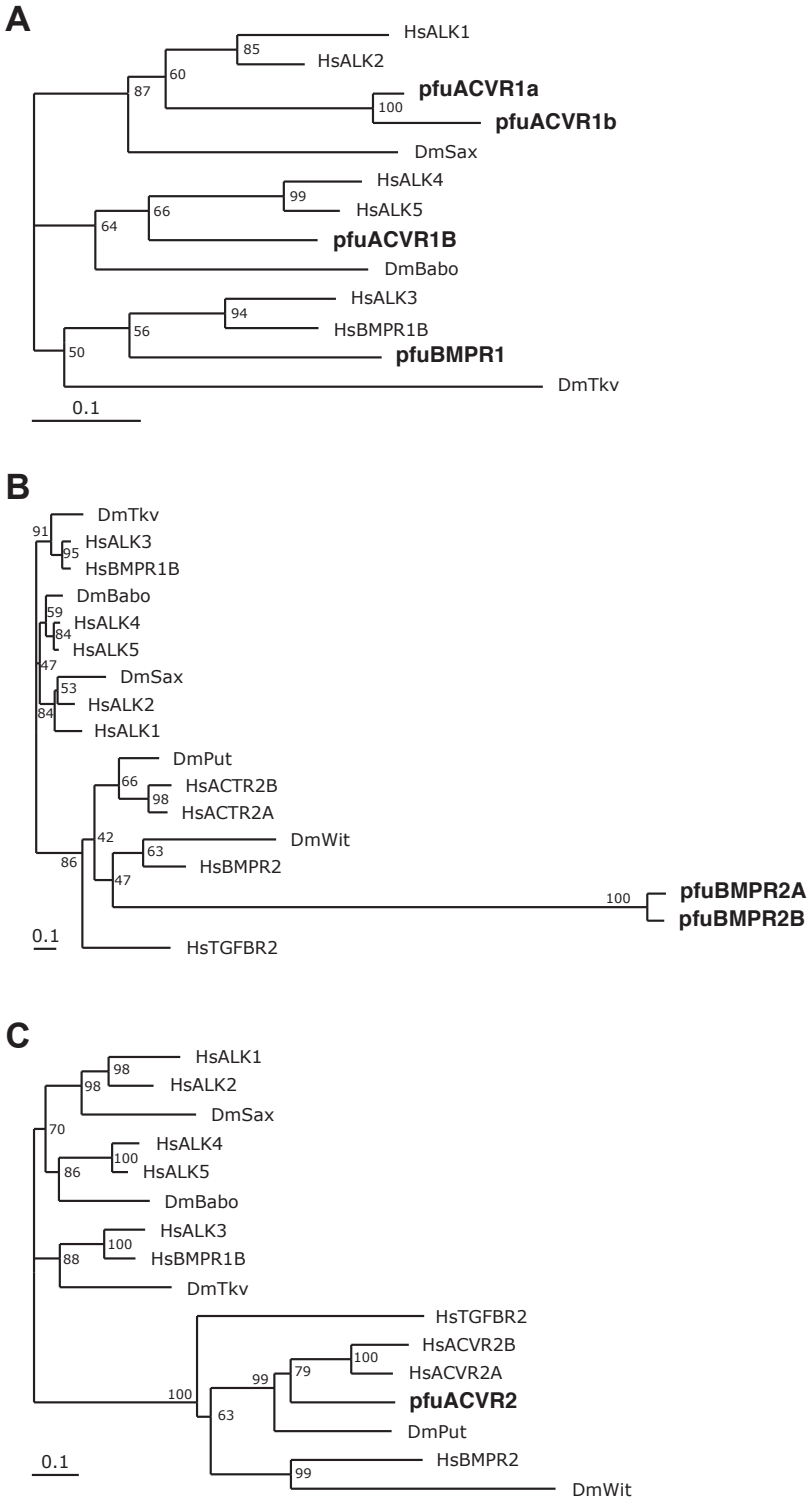

Figure 6. 3 The phylogenetic tree of TGFβ-receptors. Three Type-I receptors (**A**) and two Type-II receptors (**B and C**) were found in the pearl oyster *Pinctada fucata* genome. Homologs to all TGFβ superfamily receptor sets in *D. melanogaster* were found in mollusk. However, these predicted gene models are probably not complete sequence, lacking some parts of their domains. Bootstrap supports below 40% are not shown.

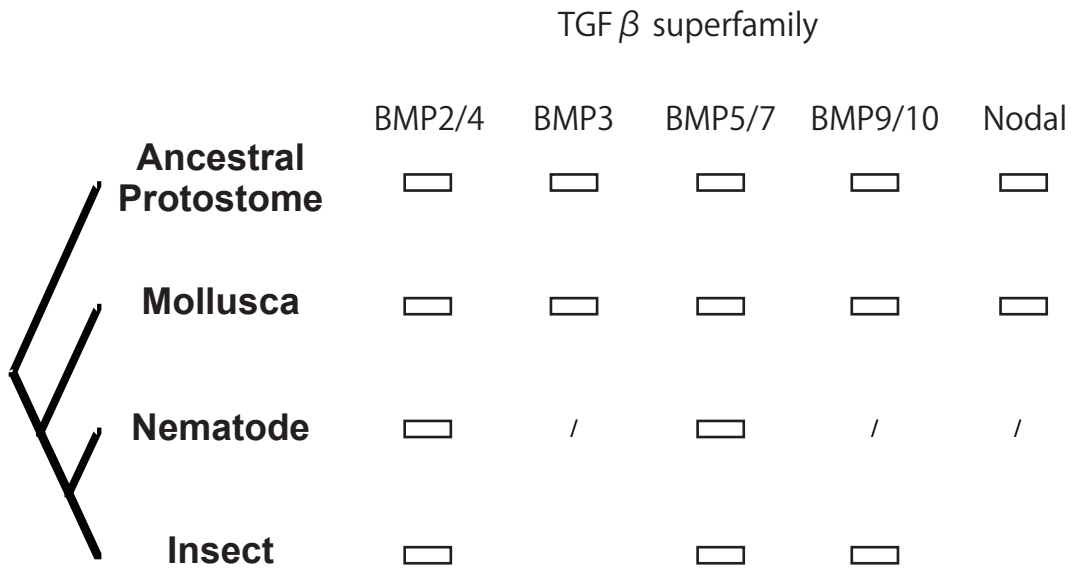

Figure 6. 4 Reconstructions of gene copy numbers of the ancestral lophotrochozoans and ancestral protostome. I assumed the greatest common factor where all gene copies present in any extant protostome must have had at least one copy in the ancestors, and if multiple copies are present in only one species, I assumed that it was duplicated locally. I also put the information of deuterostome genes into consideration. For the ancestral deuterostome, I refer to findings from the basal chordate amphioxus and other vertebrates. Question marks indicate uncertainties or lack of information; while cross marks on the ancestral protostome indicate possible absence.

6. 3. 2 Insights into the evolution of TGFβ superfamily genes in protostomes

In this report, I conducted a general survey for genes related to axis formation in early embryonic development. I then especially emphasized this survey on one of the signaling molecule ligand-coding gene families, namely TGFβ superfamily. This result allows us to predict the possible ancestral condition of the gene copy numbers in protostome, and its possible evolutionary process. In Fig. 6. 4, I present a phylogenetic character mapping for the presence/absence of TGFβ superfamily members on the protostome tree. The result suggested that the ancestral protostome had six copies of *bmp*-related genes, one copy of *activin/tgfβ* gene. Fig. 6. 4 indicates that genomes of the model ecdysozoans (*D. melanogaster* and *C. elegans*) are be possibly highly derived because of extensive local duplications and lineage specific losses. Meanwhile, this observation suggests that mollusks retain most gene copies, probably indicating that molluscan genomes are closer to that of the ancestral protostome.

Chapter Ⅶ

General Discussion

本章については、5年以内に 雑誌等で刊行予定のため、非公開。

本章については、5 年以内に 雑誌等で刊行予定のため、非公開。

本章については、5 年以内に 雑誌等で刊行予定のため、非公開。

本章については、5 年以内に 雑誌等で刊行予定のため、非公開。

本章については、5 年以内に 雑誌等で刊行予定のため、非公開。

本章については、5 年以内に 雑誌等で刊行予定のため、非公開。

本章については、5 年以内に 雑誌等で刊行予定のため、非公開。

本章については、5 年以内に 雑誌等で刊行予定のため、非公開。

本章については、5 年以内に 雑誌等で刊行予定のため、非公開。

本章については、5 年以内に 雑誌等で刊行予定のため、非公開。

本章については、5 年以内に 雑誌等で刊行予定のため、非公開。

本章については、5 年以内に 雑誌等で刊行予定のため、非公開。

References

Ackerly SC. (1989) Shell coiling in gastropods: analysis by stereographic projection. Palaios 4, 374–378.

Aktipis SW, Giriibet G, Lindberg DR, Ponder WF: Gastropoda: an overview and analysis. In *Phylogeny and Evolution of the Mollusca.* Edited by Ponder WF, Lindberg DR. University of California Press, Berkeley and Los Angeles (2008) 201–238.

Asami T, Gittenberger E, Falkner G. (2008) Whole-body enantiomorphy and maternal inheritance of chiral reversal in the pond snail *Lymnaea stagnalis*. J. Hered. 99, 552–557.

Bandel K (1990) Shell structure of the gastropoda excluding archaeogastropoda. In Carter JG (ed) Skeletal biomineralization: patterns, processes and evolutionary trends, Van Nostrand Reinhold, New York, pp 117-133.

Baratte S, Andouche A, Bonnaud L (2007) Engrailed in cephalopods: a key gene related to the emergence of morphological novelties. Dev. Genes Evol. 217, 353-62.

Barolo S, Posakony JW (2002) Three habits of highly effective signaling pathways: principles of transcriptional control by developmental cell signaling. Genes Dev. 16, 1167-1181.

Barucca M, Olmo E, Canapa A (2003) Hox and paraHox genes in bivalve molluscs. Gene 317, 97–102.

Bielefeld U, Becker W (1991) Embryonic development of the shell in Biomphalaria glabrata (Say). International Journal of Dev Bio 35, 121–131.

Biscotti MA, Canapa A, Olmo E, Barucca M (2007) Hox genes in the antarctic polyplacophoran Nuttallochiton mirandus. J. Experiment Zool. 308B, 507–513.

Brönmark, C., Lakowitz, T., Hollander, J. (2011) Predator-induced morphological plasticity across local populations of a freshwater snail. PLoS One 6 (7), e21773.

Callaerts P, Lee PN, Hartmann B, Farfan C, Choy DWY, Ikeo K, Fischbach K, Gehring WJ, de Couet HG (2002) Hox genes in the sepiolid squid Euprymna scolopes: implications for the evolution of complex body plans. Proc. Natl. Acad. Sci. USA 99 (4), 2088–2093.

Canapa A, Biscotti MA, Olmo E, Barucca M (2005) Isolation of Hox and ParaHox genes in the bivalve Pecten maximus. Gene 348, 83–88.

Cannon JE, Upton PD, Smith JC, Morrell NW (2010) Intersegmental vessel formation in zebrafish: requirement for VEGF but not BMP signalling revealed by selective and non-selective BMP antagonists. B. J. P. 161, 140-149.

Cartwright JHE, Checa AG (2007) The dynamics of nacre self-assembly. J. R. Soc. Interface 4, 491–504.

Cather, JN (1967) Cellular interactions in the development of the shell gland of the gastropod, Ilyanassa. J. Experiment Zool. 166, 205-223.

Chaikuad A, Alfano I, Shrestha B, Muniz JRC, Petrie K, Fedorov O, Phillips C, Bishop S, Mahajan P, Pike ACW, von Delft F, Muller-Knapp S, Lee WH, Marsden BD, Arrowsmith CH, Edwards AM, Weigelt J, Bountra CK, Knapp S, Bullock A (2009) Crystal structure of the kinase domain of type I activin receptor (ACVR1) in complex with FKBP12 and dorsomorphin. RCSB PDB Protein Data Bank, Worldwide Protein Data Bank. (http://www1.rcsb.org/pdb/explore.do?structureId=3H9R)

Collin R, J Voltzow (1998) Initiation, calcification, and form of larval ‘‘archaeogastropod’’ shells. J. Morphol. 235, 77–89.

Conklin, EG (1897) The embryology of Crepidula. J. Morph. 13, 1-226.

De Robertis EM, Sasai Y (1996) A common plan for dorsoventral patterning in Bilateria. Nature. 7, 380, 37-40.

DePaula SM, Huila MFG, Araki K, Toma HE (2010) Confocal Raman and electronic microscopy studies on the topotactic conversion of calcium carbonate from Pomacea lineate shells into hydroxyapatite bioceramic materials in phosphate media. Micron 983-989.

DeWitt, TJ, Sih, A., Hucko, JA (1999) Trait compensation and cospecialization in a freshwater snail: size, shape and antipredator behaviour. Anim. Behav. 58, 397–407.

DeWitt, TJ., Robinson, BW., Wilson, DS (2000) Functional diversity among predators of a freshwater snail imposes an adaptive trade-off for shell morphology. Evol. Ecol. Res. 2, 129–148.

Eyster LS, Morse MP (1984) Early Shell Formation During Molluscan Embryogenesis, with New Studies on the Surf Clam, Spisula solidissima. Amer. Zool. 24, 871-882.

Eyster LS (1986) Shell inorganic composition and onset of shell mineralization during bivalve and gastropod embryogenesis. Biol. Bull. 170, 211–231.

Fukura S, Mizukami T, Odake S, Kagi H (2006) Factors determining the stability, resolution, and pression of a conventional Raman spectrometer. Appl. Spectrosc. 60, 946-950.

Futuyma DJ (2005) Evolution. 1st edition: Evolution and Development. Sinauer Associates Inc. U.S.A. pp 473-499

Gazave E, Lapébie P, Richards GS, Brunet F, Ereskovsky AV, Degnan BM, Borchiellini C, Vervoort M, Renard E (2009) Origin and evolution of the Notch signalling pathway: an overview from eukaryotic genomes. BMC Evol. Biol. 13, 249.

Grande C, Patel NH (2009) Nodal signalling is involved in left-right asymmetry in snails. Nature 457, 1007–1011.

Hall, BK (1998). *Evolutionary Developmental Biology*. 2nd edition: Bauplane, constrains and basic phases of development. Kluwer Academic Publishers, Dordrecht. Netherlands. pp 93-109.

Hammer O, Bucher H (2005) Models for the morphogenesis of the molluscan shell. Lethaia, 38, 111–122.

Hashimoto N, Kurita Y, Wada H (2012) Developmental role of *dpp* in the gastropod shell plate and co-option of the *dpp* signaling pathway in the evolution of the operculum. Dev. Bio. 366, 367–373.

Hinman VF, O'Brien EK, Richards GS, Degnan BM (2003) Expression of anterior Hox genes during larval development of the gastropod Haliotis asinina. Evol. Dev. 5, 508–521.

Huminiecki L, Goldovsky L, Freilich S, Moustakas A, Ouzounis C, Heldin CH (2009) Emergence, development and diversification of the TGFβ signaling pathway within the animal kingdom. BMC Evol. Biol. 9, 28.

Iijima M, Takeuchi T, Sarashina I, Endo K (2008) Expression patterns of engrailed and dpp in the gastropod Lymnaea stagnalis. Dev. Genes. Evol. 218, 237-51.

Jacobs DK, Wray CG, Wedeen CJ, Kostiken R, Desalle R, Staton JL, Gates RD, Lindberg DR (2000) Molluscan engrailed expression, serial organization, and shell evolution. Evol. Dev. 2, 340-347.

Jardillier E, Rousseau M, Gendron-Badou A, Frohlich F, Smith DC, Martin M, Helleouet MN, Huchette S, Doumenc D, Auzoux- Bordenave S (2008) A morphological and structural study of the larval shell from the abalone Haliotis tuberculata. Mar. Biol. 154, 735–744.

Kin K, Kakoi S, Wada H (2009) Novel role for dpp in the shaping of bivalve shells revealed in a conserved molluscan developmental program. Dev. Biol. 329, 152–166.

Kinoshita S, Wang N, Inoue H, Maeyama K, Okamoto K, Nagai K, Kondo H, Hirono I, Asakawa S, Watabe S (2011) Deep sequencing of ESTs from nacreous and prismatic layer producing tissues and a screen for novel shell formation-related genes in the pearl oyster. PLoS One 6, e21238.

Knight JB, Cox LR, Keen AM, Batten RL, Yochelson EL, Robertson R (1960) *Systematic descriptions* (*Archaeogastropoda*). In *Treatise on Invertebrate Paleontology. Part I. Mollusca.* Edited by Moore RC. Geol. Soc. Amer. and Kansas Univ. Press, 1, 169–310.

Kniprath, E (1981) Ontogeny of the molluscan shell field. Zoologica. Scripta. 10, 61–79.

Kocot KM, Cannon JT, Todt C, Citarella MR, Kohn AB, Meyer A, Santos SR, Schander C, Moroz LL, Lieb B, Halanych KM (2011) Phylogenomics reveals deep molluscan relationships. Nature 477, 452-456.

Kojima S (1997) Paraphyletic status of polychaeta suggested by phylogenetic analysis based on the amino acid sequences of elongation factor-1 alpha. Mol. Phy. Evo. 9, 255–261.

Koop D, Richards GS, Wanninger A, Gunter HM, Degnan BM (2007) The role of MAPK signaling in patterning and establishing axial symmetry in the gastropod Haliotis asinina. Dev. Biol. 311, 200-212.

Kurita Y, Wada H (2011) Evidence that gastropod torsion is driven by asymmetric cell proliferation activated by TGF-ß signaling. Biol. Lett. 7, 759–762.

Kuroda R, Endo B, Abe M, Shimizu M (2009) Chiral blastomere arrangement dictates zygotic left-right asymmetry pathway in snails. Nature 462, 790-794.

Lambert JD, Nagy LM (2002) Asymmetric inheritance of centrosomally localized mRNAs duringembryonic cleavages. Nature 420, 682-686.

Lemche H (1957) A new living deep-sea mollusc of the Cambro-Devonian class Monoplacophora. Nature 179, 413–416.

Letunic I, Doerks T, Bork P (2012) SMART 7: recent updates to the protein domain annotation resource. Nucl. Acids. Res. 40, D302-D305.

Lewis EB (1978) A gene complex controlling segmentation in Drosophila. Nature 276, 565–570.

Lowe CJ, Wray GA (1997) Radical alterations in the roles of homeobox genes during echinoderm evolution. Nature 389, 718-721.

Lowe LA, Yamada S, Kuehn MR (2001) Genetic dissection of nodal function in patterning the mouse embryo. Development 128, 1831-1843.

Maddison WP, Maddison DR (2011) Mesquite: a modular system for evolutionary analysis. Version 2.75 http://mesquiteproject.org

Meshcheryakov VN (1990) The common pond snail Lymnaea stagnalis. In: Dettlaff TA and Vassetzky SG (eds) Animal Species for the Developmental Studies, Consultants Bureau, New York, pp 69-132.

Morill JB (1982) Development of the pulmonate gastropod, “Lymnaea”. In: Harrison FW, Cowden RR (eds) Developmental biology of fresh water invertebrates. Alan R Liss Inc, New York, pp 399–483.

Moshel SM, Levine M, Collier JR (1998) Shell differentiation and engrailed expression in the Ilyanassa embryo. Dev. Genes Evol. 208, 135-141.

Nederbragt AJ, van Loon AE, Dictus WJ (2002) Expression of Patella vulgata orthologs of engrailed and dpp-BMP2/4 in adjacent domains during molluscan shell development suggests aconserved compartment boundary mechanism. Dev. Biol. 246, 341-355.

Nellen D, Burke R, Struhl G, Basler K (1996) Direct and longrange action of a DPP morphogen gradient. Cell, 85, 357–368.

Okamoto T (1988) Analysis of heteromorphy ammonoids by differential geometry. Palaeontology 31, 35–52.

Palmer AR (1979) Fish predation and the evolution of gastropod shell sculpture experimental and geographic evidence. Evolution 33, 697–713.

Patel NH, Martin-Blanco E, Coleman KG, Poole SJ, Ellis MC, Kornberg TB, Goodman CS (1989) Expression of engrailed proteins in arthropods, annelids and chordates. Cell 58, 955–968.

Pei J, Kim BH, Grishin NV (2008) PROMALS3D: a tool for multiple sequence and structure alignment. Nucleic. Acid. Res. 36, 2295-2300.

Pérez-Parallé ML, Carpintero P, Pazos A, Abad M, Sánchez J (2005) The HOX gene cluster in the bivalve mollusc Mytilus galloprovincialis. Biochem. Genet. 43, 417–424.

Pernice M, Deutsch JS, Andouche A, Boucher-Rodoni R, Bonnaud L (2006) Unexpected variation of Hox genes' Homeodomains in Cephalopods. Mol. Phylogenet. Evol. 40, 872–879.

Pires-daSilva A, Sommer RJ (2003) The evolution of signalling pathways in animal development. Nat. Rev. Genet. 4, 39-49.

Ponder WF, Lindberg DR (1997) Towards a phylogeny of gastropod molluscs: an analysis using morphological characters. Zool. J. Linn. Soc. 119, 88–265.

Raup DM (1966) Geometric analysis of shell coiling: general problems. J. Paleontlogy 44, 1178–1190.

Rice SH (1998) The bio-geometry of mollusc shells. Paleobiology 24, 133–149.

Rogulja D, Irvine KD (2005) Regulation of cell proliferation by a morphogen gradient. Cell 123, 449–461.

Runnegar B (1996) Early evolution of the mollusca: The fossil record. In: Taylor JD (ed), Origin and Evolutionary Radiation of the mollusca, Oxford, pp. 77–87.

Savazzie E (1990) Biological aspects of theoretical shell morphology. Lethaia 23, 195-212.

Setiamarga DH, Shimizu K, Kuroda J, Inamura K, Sato K, Isowa Y, Ishikawa M, Maeda R, Nakano T, Yamakawa T, Hatori R, Ishio A, Kaneko K, Matsumoto K, Sarashina I, Teruya S, Zhao R, Satoh N, Sasaki T, Matsuno K, Endo K. (2013) An in-silico genomic survey to annotate genes coding for early development-relevant signaling molecules in the pearl oyster, *Pinctada fucata*. Zool. Sci. 30, 877-888.

Shigeno S, Sasaki T, Moritaki T, Kasugai T, Vecchione M, Agata K (2008) Evolution of the cephalopod head complex by assembly of multiple molluscan body parts: Evidence from nautilus embryonic development. J. Morphol. 269, 1-17.

Shimizu K, Sarashina I, Kagi H, Endo K. (2011) Possible functions of Dpp in gastropod shell formation and shell coiling. Dev. Genes Evol. 221, 59-68.

Shimizu K, Iijima M, Setiamarga DH, Sarashina I, Kudoh T, Asami T, Gittenberger E, Endo K. (2013) Left-right asymmetric expression of dpp in the mantle of gastropods correlates with asymmetric shell coiling. Evodevo 4, 15.

Shimozono S, Iimura T, Kitaguchi T, Higashijima S, Miyawaki A. (2013) Visualization of an endogenous retinoic acid gradient across embryonic development. Nature 496, 363-366.

Stone JR (1995) CerioShell: a computer program designed to simulate variation in shell form. Paleobiology 21, 509–519.

Tollrian, R (1990) Predator-induced helmet formation in Daphnia cucullata (Sars). Arch. Hydrobiol. 119, 191–196.

Tollrian R and Dodson S (1999) Inducible defenses in Cladocera: Constraints, costs, and multipredator environments. In Tollrian, R. and Harvell, C. D. (eds), The Ecology and Evolution of Inducible Defenses. Princeton University Press, Princeton, pp. 177–202.

Wanninger A, Haszprunar G (2001) The expression of an engrailed protein during embryonic shell formation of the tusk-shell, *Antalis entalis* (Mollusca, Scaphopoda). Evol. Dev. 3, 312-321.

Weismann A (1875) Über den saison-dimorphismus der schmetterlinge. In “Studien zur Descendenz-Theorie.” Engelmann, Leipzig.

West-Eberhard MJ (1989) Phenotypic plasticity and the origins of diversity. Annu. Rev. Ecol. Syst. 20, 249–278.

Acknowledgements

I am deeply grateful to Prof. Kazuyoshi Endo (Department of Earth and Planetary Science, The University of Tokyo) as my academic advisor during my doctorate study. Without his numerous and valuable suggestions and continuous encouragement, this study could not be finished.

I am very grateful to Associate Prof. Takenori Sasaki (The University Museum, The University of Tokyo) for invaluable discussion and advice on this study and providing me with some shell photographs. I also really appreciate Associate Prof. Rei Ueshima (Department of Biological Science, The University of Tokyo), Prof. Satoshi Chiba (Department of Environmental Life Sciences, Tohoku University), Dr. Takanobu Tsuihiji (Department of Earth and Planetary Science, The University of Tokyo) for valuable comments and advice.

I am grateful to Prof. Hiroyuki Kagi, Dr. Isao Sarashina, Dr. Davin HE Setiamarga (Department of Earth and Planetary Science, The University of Tokyo), Dr. Tetsuhiro Kudoh (University of Exeter) and Dr. Minoru Iijima (University of Tsukuba) for invaluable discussion and participation in the design and coordination of my study. I also very much appreciate Prof. Takahiro Asami (Shinshu University) and Prof. Edi Gittenberger (Naturalis Biodiversity Center) for their generous gift of the dextral and sinistral strains of the pond snail *Lymnaea stagnalis*. I really thank Prof. Kenji Matsuno, Dr. Junpei Kuroda (University of Oosaka), for discussion, suggestions and help in functional analysis of Dpp. I would like to thank Prof. Noriyuki Sato, Dr. Takeshi Takeuchi (Okinawa Institute Science and Technology Graduate University), Dr. Reo Maeda, Dr. Tomoko Yamakawa, Mr. Ryo Hatori, Mr. Akira Ishio, Mr. Kenjiroo Matumoto, Ms. Kayo Kaneko (University of Oosaka), Dr. Tomoyuki Nakano (University of Kyoto), Mr. Yukinobu Isowa, Mr. Kengo Inamura, Mr. Kei Satoh, Mr. Shinnosuke Teruya, Mr. Zhao Ran (The University of Tokyo) for participation in the pearl oyster genome jamboree and valuable discussion and advice.

I would like to thank Prof. Hiroshi Wada, Naoki Hashimoto (University of Tsukuba) and Yoshihisa Kurita (University of Kyushu) for the gift of the adult specimens of *N. fuscoviridis* and for discussion, suggestions and help in functional analysis of Dpp. I would like to thank Koji Noshita (University of Kyushu) for useful discussion about mathematical models. I would like to thank Dr. Michinari Sunamura (University of Tokyo) and Dr. Katsunori Yanagawa (Japan Agency for Marine-Earth Science and Technology) for help with qRT-PCR

analysis. I would like to thank Dr. Michio Suzuki, Dr. Makiko Ishikawa (The University of Tokyo), Dr. Aya Takesono, Dr. Sulayman Mourabit and Dr. Yujirou Higuchi (University of Exeter) for help with protein analysis. I would like to thank Associate Prof. Toshihiro Kogure, Koji Ichimura and Naoki Yokoo (The University of Tokyo) for help with compositional analysis of the shell.